2005

Electron stimulated desorption of hydronium ions from chromium oxide surfaces

Charles Randal Cole
College of William & Mary - Arts & Sciences

ELECTRON STIMULATED DESORPTION OF HYDRONIUM IONS FROM CHROMIUM OXIDE SURFACES

A Dissertation

Presented to

The Faculty of the Department of Applied Science

The College of William and Mary in Virginia

In Partial Fulfillment

Of the Requirements for the Degree of

Doctor of Philosophy

---

by

Charles Randal Cole

2005

APPROVAL SHEET

This dissertation is submitted in partial fulfillment of

the requirements for the degree of

Doctor of Philosophy

Charles Randal Cole

Charles Randal Cole

Approved by the Committee, December 2005

Brian C. Holloway, Chair

Ronald A. Outlaw

Roy L. Champion
Department of Physics

J. C. Poutsma
Department of Chemistry

Anne C. Reilly
Department of Physics

To Mom and Dad

TABLE OF CONTENTS

Page

ACKNOWLEDGEMENTS

I want to first thank my Lord Jesus Christ for the strength and patience to undertake this endeavor, and for the opportunity to explore His creation on a scale beyond what the eye can see. "For by Him were all things created, that are in heaven, and that are in earth, visible and invisible, whether they be thrones, or dominions, or principalities, or powers: all things were created by Him, and for Him: And He is before all things, and by Him all things consist." - *Colossians 1:16-17.*

I thank my family and friends for their interest and encouragement along the way. It has helped immensely.

I would certainly like to thank the members of my committee: Dr. Ronald Outlaw, Dr. Roy Champion, Dr. J.C. Poutsma and Dr. Anne Reilly. And, of course, I express great appreciation to my advisor Dr. Brian Holloway for his guidance and support over the course of this research.

I thank several people who have contributed at different points during this work: Dr. Doug Baker at Teledyne Hastings Instruments for his guidance using vacuum technology, Amy Wilkerson and Christine Hopkins for assistance with the TOF SIMS at the Applied Research Center of Jefferson Lab, Hui Tian for help with the W&M XPS system and Dr. Michael Kelly for the use of the XPS at Stanford University. I also thank the late Dr. Paul Redhead for discussions during the course of this research.

I would like to acknowledge the support provided by Virginia's Center for Innovative Technology (CIT) and by the Division of Chemical Sciences, Office of Basic Energy Science, USDOE.

And, finally, I greatly appreciate the flexibility given to me by Teledyne Hastings Instruments over these several years to complete this work.

LIST OF TABLES

LIST OF FIGURES

ABSTRACT

The mass spectral peak observed at 19 amu in residual gas analyzers at very high (< 10^{-6} Torr) and ultrahigh vacuum (< 10^{-9} Torr) has often been attributed to fluorine. Using Fourier Transform Mass Spectrometry, the hydronium ion, H_3O^+, has been fully resolved from F^+ and its correlation to water vapor concentration was determined to be linear as expected for a gas phase process. The comparison of the mass 19 signals for a conventional quadrupole mass spectrometer and a Fourier transform mass spectrometer on the same vacuum chamber indicated hydronium was the source of mass 19.

The partial pressures of H_2O in the very high vacuum range and higher suggest there is sufficient H_2O density for the hydronium ions to form through ion-molecule interactions because hydronium formation was found to directly correlate with the H_2O partial pressure. However, in a QMS at UHV, formation of H_3O^+ appears to occur principally by electron stimulated desorption (ESD). Introducing hydrogen into the system from 1 Langmuir exposure to saturation (1×10^{-6} Torr for 8 hours) increased the H_3O^+ ESD yield detected by the QMS by as much as a factor of 10. The initial hydronium ESD cross section from a hydrogen saturated grid was estimated to be $\sigma \sim 1 \times 10^{-19}$ cm^2.

TOF-SIMS sputter yields from the stainless steel grid of a quadrupole mass spectrometer also showed small signals of H_3O^+, as well as its constituents (H^+, O^+ and OH^+) and a small amount of fluorine as F^-, but no F^+ or F^+ complexes (HF^+, etc.). Using x-ray photoelectron spectroscopy, a small amount (0.4%) of fluorine was found in the surface of stainless steel. Electron bombardment reduces the fluorine bound in surface complexes, but not metal halides found below the surface. However, heating the sample eliminated the F 1s signal entirely, indicating that fluorine is not likely to be the source of mass 19 in residual gas analysis. Also, changes in the spectral shoulders on the O 1s and Cr $2p_{3/2}$ peaks show that hydrogen dosing stainless steel and chromium increases the amount of hydroxides at the surface, while heating and electron bombardment reduce them.

ELECTRON STIMULATED DESORPTION OF HYDRONIUM IONS FROM CHROMIUM OXIDE SURFACES

CHAPTER I

INTRODUCTION

1.1 Background

The vacuum technology industry has grown tremendously as advances have been made in the semiconductor industry and in materials science. Smaller semiconductor devices, thin film materials, innovative nanotechnology and micro-electromechanical devices have required simultaneous advances in vacuum technology, low pressure physics and surface science. In order to study surfaces thoroughly and develop new technology, one needs to have a low pressure environment ($< 10^{-8}$ Torr) where few molecules remain to interact with those surfaces. Even at such low pressures, molecules still enter the vacuum from contamination on the chamber walls or after having been dissolved in the metal walls themselves. This residual gas background can affect the surfaces or processes of interest.

1.1.1 Anomalous Peaks in Mass Spectra - ESD

It is important to know what the low pressure environment of a vacuum chamber contains because the residual gas or impurities can be incorporated into devices and materials as they are being made or studied. For a semiconductor

fabrication plant, this could mean the loss of an entire batch of silicon wafers and millions of dollars. For a materials scientist, this could give erroneous data or change the expected properties of a new sample.

Mass spectrometry gives an indication of what types of atoms and molecules exist in a vacuum environment. It can give an indication of contaminants in a system, whether there is a leak or if a gas mixing process is correct. The molecules of interest ultimately end up in the gas phase, where they can be ionized in the ion source of a mass spectrometer.

A number of different mass spectrometers have been developed to analyze the ions. Magnetic sector types use the fact that charged particles follow different curved paths in a magnetic field, depending on their mass. Quadrupole mass spectrometers (QMS) use an oscillating electric field that allows particles of a particular mass to pass through to a detector. Normally, the detection is done by either measuring the ion current directly or by having the ions strike an electron multiplier and measuring the amplified current.

After detection, the ion current can be plotted corresponding to what mass was allowed to pass, yielding the peaks of a mass spectrum. There are many instances where a peak in a mass spectrum arises and it is difficult to readily identify the elemental composition or its source. For example, some ions originate from surfaces during electron bombardment and may not be associated with a typical residual gas. If an ion is suspected to be fragment of a larger molecule, libraries of mass spectra can be consulted to determine what it might be. However, sometimes molecules have

mass numbers that are so close to each other that traditional mass spectrometers cannot differentiate between them, such as CO (27.995 amu) and N_2 (28.006 amu).

Using high resolution residual gas analysis, such as Fourier Transform Mass Spectrometry (FTMS) and time of flight (TOF) techniques, the confusion about the composition of a particular mass signal can be resolved. Early research has shown that a peak commonly attributed to one atom or molecule is actually made up of two or more species of slightly different mass. Mass 28 is often actually CO^+, N_2^+ and $C_2H_4^+$. Masses 15 and 16 are not just CH_3^+ and CH_4^+, but also NH^+ and NH_2^+. Indeed, NH_3^+ is seen with OH^+ and H_3O^+ is seen with F^+ at 17 and 19, respectively, in a 10^{-7} Torr diffusion pumped system.[1]

1.2 Pursuing FTMS Resolution of H_3O^+ and F^+

In particular, it is not unusual for mass 19 to appear in the output of a mass spectrometer.[2] There are many possible species (see Table 1.1) that could be responsible for such a gas-phase signal.[3] Normally this signal is attributed to the presence of fluorine[4-7]* (18.998 amu), which is a reasonable assignment since there are numerous sources of fluorine in some vacuum systems, such as pump oils, elastomer seals and solvents. However, there are significant reasons to believe the signal is not fluorine. First, most residual gas analyzers only detect positive ions, and it is difficult to form positive ions of fluorine because it is the most electronegative element (electron affinity = 3.4 eV). Second, many fluorine-containing gases are also

* Ellefson, p.472; O'Hanlon, pp. 152,221,312; Drinkwine, p.57

electronegative and show a fragmentation pattern with the largest peak at the mass number corresponding to having one fluorine dissociatively removed. For example, SF_6 does not have a significant peak at mass 19 in its positive ion spectrum. Also, most modern ultra high vacuum systems utilize very few elastomers or pump oils, but the mass 19 peak is still often quite prevalent.

Other isotopes of oxygen or hydrogen could also account for the signal at mass 19 amu. However, the signal is generally greater than 2% of the mass 18 signal (H_2O), while established isotopic ratios are 0.02% for deuterium and 0.038% and 0.205% for oxygen isotopes ^{17}O and ^{18}O respectively.[8] Clearly, these cannot account for such a large signal at 19 amu.

While most commercial quadrupole mass spectrometer (QMS) instruments cannot resolve peaks extremely close in mass (for example the mass difference between H_3O^+ and F^+ is $\Delta m = 0.02$ amu), Fourier transform mass spectrometry, also known as Fourier transform ion cyclotron resonance (FTICR) mass spectrometry, has the very high resolution required to differentiate between gas species with similar mass numbers. This technique detects the motion of ions confined by a set of electrodes located in a strong, uniform magnetic field. As the ions move, they induce an image current in the electrodes that is then amplified. This signal contains all the frequencies corresponding to ion masses, each with an amplitude related to the number of ions of that mass. The frequencies are separated by performing a Fourier transform on the signal, resulting in a mass spectrum.

FTMS usually uses very high magnetic fields (over 1 T) in order to obtain mass spectral data of large molecules, such as proteins that are of interest in biology

and pharmacology. As magnetic field strength increases, so does the resolving power ($m/\Delta m$) of the instrument. Some instruments have resolving power greater than 10^6.

TABLE 1.1 Molecules at approximately 19 amu.[3]

Molecule	Mass
F	18.99840320
$H^{18}O$	19.00698543
$D^{17}O$	19.01323328
$H_2{}^{17}O$	19.01478156
$HD^{16}O$	19.01684143
$H_3{}^{16}O$	19.01838972
$^{15}ND_2$	19.02831245
$^{15}NH_2D$	19.02986074
$^{15}NH_4$	19.03140903
$^{14}NHD_2$	19.03910259
$^{14}NH_3D$	19.04065088
$^{13}CD_3$	19.04566017
$^{13}CH_2D_2$	19.04720846
$^{12}CHD_3$	19.05013037

1.3 Measuring Gas Phase H_3O^+

An alternative to fluorine as the source of the mass 19 signal is the formation of hydronium (H_3O^+) ions (19.018 amu). It is well known that hydronium is present in liquid water and that proton exchange between water molecules occurs quite frequently. There are also a number of gas-phase reactions that can lead to the formation of hydronium, including:

$$H_2O^+ + H_2O \rightarrow H_3O^+ + OH \qquad (1.1)$$

Realizing that water vapor is a major constituent of many vacuum systems, it is helpful to consider how hydronium formation occurs in the gas phase. However, some researchers have suggested that hydronium cannot be a significant contributor to the mass 19 signal at ultrahigh vacuum because of the lack of water in these systems.[9] Even when water was introduced into the vacuum system causing the mass 19 signal to increase, the water purity was questioned (fluorine contamination) rather than considering hydronium to be the source.[9] Fortunately, the gas phase formation of hydronium can be studied using the FTICR mass spectrometer because ionization times and reaction times can be adjusted within the spectrometer.

1.4 Pursuing an ESD Mechanism for H_3O^+ Generation

Ion energy distribution experiments by Adrados[9] and Neave[10] have shown that the mass 19 peak is most likely due to electron stimulated desorption from the grid of the ion source of the mass spectrometer. Since ESD ions have slightly more kinetic energy and come from different points within the ionizer compared to ions formed in the gas phase, it has been possible to differentiate the origins by varying electrode potentials in mass spectrometers. The general consensus is that fluorine may exist throughout the bulk of many metals, much like hydrogen, except with lower concentrations.[11] Impurities can be incorporated from metal halides in the air,[12] Freon cleaning agents,[13] or ions in rinse water or in moisture from

human hands. Thermal desorption spectroscopy[14] and secondary ion mass spectrometry (SIMS) has shown sodium, chlorine and potassium[12,13,15] to be present in stainless steel as well as other metals (W, Re), but the amount of these metal halides at the surface is not as great as that of oxygen or hydrogen.

While there are reasons to consider fluorine to be the source, hydronium must also be considered. Hydronium generation through surface processes has been observed in early field desorption experiments[16] and more recently through the ESD mechanism.[17] Generation of hydronium by ESD, though suggested,[10] has not been examined extensively. It is interesting to consider, then, the formation of hydronium in the ion source of a QMS. The effects of dosing with hydrogen should give insight into the processes involved.

1.5 TOF SIMS and XPS Characterization of Stainless Steel

Because anomalous peaks in mass spectra seem to originate from surface species, it is helpful to use other surface analysis techniques to gain additional insight. Time of flight secondary ion mass spectrometry (TOF SIMS) is an extremely surface sensitive technique that can resolve 0.001 amu. The technique has been used to study stainless steel composition and surface chemistry,[11,18] which is of particular interest since the grid of many ion sources are made of this material. The act of bombarding the sample during TOF SIMS analysis leads to thermal surface desorption. As the ions bombard the surface, they transfer their momentum to the surface atoms, but they can also cause ion stimulated desorption (ISD). This type of

desorption occurs much like ESD, through induced electronic transitions. Any atoms that desorb by ESD could be expected to desorb through ISD, though the extent of the comparison may be limited. Nevertheless, this technique gives a general idea of the surface composition and the propensity of the constituents to form positive or negative ions.

SIMS spectra have shown that there are atoms of Na and K in stainless steel, and this is actually common for other metals like W and Re as well.[12] Since Na is present, it could be expected to be an ESD product as much as fluorine. As an electropositive element, it would normally exist as a positive ion having small enough size to diffuse, much like a fluorine atom would. Na vapor has been seen in the sparse atmosphere of Mercury and the Moon, presumably from solar photons and electrons bombarding the surface causing PSD and ESD.[19] However, Na^+ is not usually seen in residual gas spectra from vacuum systems, further calling into question the assignment of the mass 19 signal to F^+.

X-ray photoelectron spectroscopy (XPS) is another technique that provides information about surface composition and the chemical state of the constituents. XPS has been used to show that the surface of stainless steel forms oxides and hydroxides.[18] These species could be the source of hydronium ions seen in mass spectra. Sample preparation can affect surface chemistry, as can processing. By noting changes in spectral peak shapes and locations, the composition and surface chemistry can be observed before and after heating and electron bombardment of the sample. For instance, reduction of the peak shoulder corresponding to O bound to H

indicates the loss of OH or H. XPS also reveals information about the fluorine content and how it changes after different processes.

We see that anomalous peaks in mass spectra can lead to confusion in the analysis of residual gases. It is therefore useful to attain better resolution of these peaks and explore their origin and behavior. This dissertation shows that mass 19, in particular, can be resolved and can be assigned primarily to hydronium in very high and ultra high vacuum. The behavior of this peak in a quadrupole mass spectrometer is explored and the effects of hydrogen dosing are considered. Surface analysis is also performed in order to discover more about the source of the mass 19 signal. Since fluorine and hydronium are potential sources of mass 19, we now look to the literature about the behavior of these species and how they may interact with surfaces.

CHAPTER II

THEORY AND LITERATURE SURVEY

In order to further understand how the anomalous peak at mass 19 amu may arise in mass spectra, we must explore how atoms, molecules and electrons interact with surfaces. It is useful to know what research has shown about desorption of fluorine, the formation of hydronium and the interaction of water with surfaces. It is also helpful to understand the surface science of stainless steel because this material is prevalent for components of vacuum systems. In this chapter we look at these and other related topics.

2.1 Adsorption and Desorption

Even in ultrahigh vacuum conditions, the surface of a material is not pristine. There is still a residual gas background in the vacuum system that impinges upon the surface. The particle flux, Γ, that strikes a unit surface is given by the relation

$$\Gamma = nv/4 \qquad (2.1)$$

where n is the particle density and v is the average velocity. Once these gas molecules strike the surface a number of processes can occur. The gas particles could be

diffusely or specularly scattered or be adsorbed on the surface. Subsequently, they could be incorporated into the bulk.

The gas molecules that are adsorbed may be either physisorbed or chemisorbed. Both processes may require some activation energy in order to occur. Physisorbed gas molecules are bound to the surface through weak van der Waal's forces with energies less than 40 kJ/mol (< 0.40 eV). Chemisorbed molecules are more strongly bound and desorb slowly unless energy is applied through heat or bombardment by electrons, photons, atoms or ions.

For example, hydrogen is strongly chemisorbed to metal surfaces with binding energies of 160 kJ/mol (1.66 eV). Water that first adsorbs on a metal surface is bound with a binding energy of about 96 MJ/kg-mole (1.00 eV). Water molecules bound to other water molecules in subsequent layers have a binding energy of 40.6 MJ/kg-mole (0.42 eV).[5]*

Assuming that all molecules stick to the surface as they arrive and occupy an area of d_o^2, the time required to saturate the surface with one layer of molecules (monolayer) is given by

$$t_{ml} = \frac{1}{\Gamma d_o^2} = \frac{4}{nvd_o^2} \qquad (2.2)$$

When species desorb from a surface via thermal processes, they may leave via first or second order processes. First order desorption involves atoms or molecules that desorb directly from their bound state (no recombination). They desorb at a rate

* O'Hanlon, pp.58-59

that is proportional to their surface concentration. First order desorption can be described by the equation

$$\frac{dC(t)}{dt} = -k_1 C(t) = -\frac{e^{-E_d/(k_B T)}}{\tau_0} C(t) \qquad (2.3)$$

where C(t) is the concentration of molecules on the surface as a function of time. k_1 is a rate constant that is dependent on the desorption energy, E_d, the temperature, T, Boltzmann's constant, k_B, and the residence time of a molecule in an adsorption site τ_o. K_1 is the reciprocal of the average residence time, τ_r, that a molecule stays on the surface. Using this substitution and integrating yields

$$\frac{dC(t)}{dt} = C_0 k_1 e^{-K_1 t} = C_0 k_1 e^{-t/\tau_r} \qquad (2.4)$$

where C_o is the initial concentration.

Second order desorption involves molecules that recombine before desorbing. Examples would be H_2 and CO. The desorption process involves a reaction which is proportional to the concentrations of each of the two species.[5]* Second order desorption can be described by the equation

$$\frac{dC(t)}{dt} = -k_2 C(t)^2 = \frac{-k_2 C_0^2}{(1 + C_0 k_2 t)^2} \qquad (2.5)$$

* O'Hanlon, p.59

where k_2 is of the same form as k_1. In the case of second order desorption, the time required to clean a surface is longer since the rate decays as $1/t^2$.

2.2 Electron Stimulated Desorption

Desorption can also be induced by electronic transitions through photon excitation and atom or electron bombardment. Electron stimulated desorption (ESD) generally refers to the release of adsorbed species as energetic neutral and ion fragments due to electronic excitations (as opposed to thermal effects) by low energy electrons (< 500 eV). ESD phenomena are physical and chemical effects that occur during bombardment, including bond alteration and surface decomposition. The angular distribution of ions from electron stimulated desorption can also be used to understand bond directions since the positive ions are often ejected in beams depending on their surface orientation.[20]

For a species of surface concentration C(t), first order desorption is described by

$$\frac{dC(t)}{dt} = - nQC(t) \qquad (2.6)$$

where C(t) is the coverage of adsorbed species ($1/cm^2$) in the particular binding state involved, n is the electron flux ($1/cm^2sec$) and Q is the cross-section (cm^2). In terms of ion desorption current,

$$i^+ = I_e Q^+ C(t) \qquad (2.7)$$

where i^+ is the ion current (A), I_e is the bombarding electron current (A) and Q^+ is the ionic desorption cross-section (cm^2). The particular binding states of the adsorbed species are differentiated by their activation energies.[20] Typical thresholds for ESD are in the range of 5 to 20 eV. Typical cross-sections for ion desorption from weakly bound states are ~10^{-18} cm^2 and for neutral desorption ~10^{-16} cm^2. [21]

The Menzel-Gomer-Redhead[22,23] (MGR) model for ESD proposes that an incident electron excites a bonding electron in an adsorbed atom to a nonbonding or anti-bonding state. The effective potential between the adsorbed atom and the surface atom becomes repulsive and the atom is able to desorb in either the neutral or an ionized state. An energy diagram of this process is shown in Figure 2.1. The ESD neutral gas flux can be as high as 10^{-1} atom per incident electron while the flux of desorbed ions is much smaller, on the order of 10^{-5} ion per incident electron.[5]*

The MGR process depends on the manner in which a molecule is bound to the surface; hence, some molecules are not desorbed by this process. For highly electronegative atoms, such as oxygen, an unlikely large charge transfer of 2 or 3 electrons between surface atoms could be required for oxygen desorption to be explained by the MGR mechanism.

* O'Hanlon, p.66

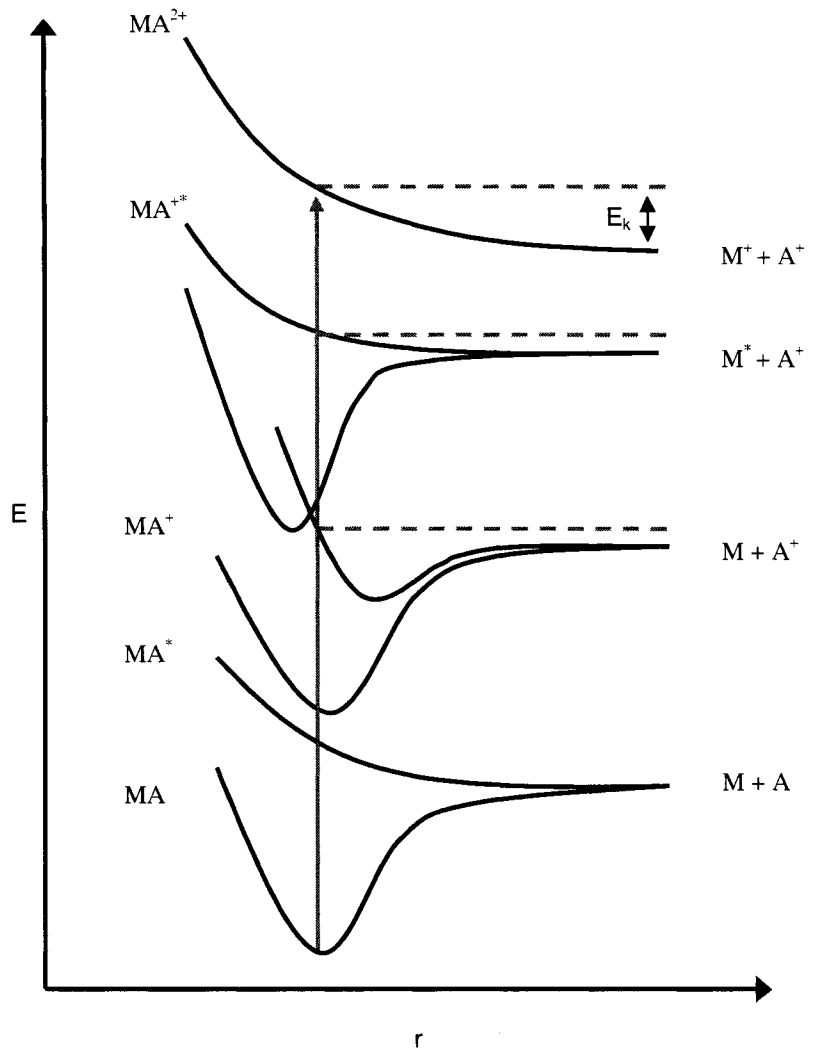

FIGURE 2.1 A potential energy diagram of the MGR ESD process shows that an adsorbate atom (A) can be excited to a non-bonding state leading to desorption with kinetic energy E_k from a substrate atom (M).

Knotek and Feibelman[24] (KF) presented an Auger decay mechanism to explain thresholds and charge transfer involved in ESD. A core hole is first created by the incident electron and this hole is filled by an Auger electronic transition. The electron comes from a higher orbital in either the adsorbed atom (intra-atomic transition) or a substrate atom (inter-atomic transition). This process is shown in

Figure 2.2. The Auger transition leaves the atom in a charged state that is repulsive to the substrate material. The new ion then desorbs via Coulombic repulsion.

An inter-atomic Auger transition is slower than an intra-atomic transition, so O^+ desorption via the KF process would be more likely to occur in maximum valence oxides (TiO_2, WO_3) where there are no valence electrons left on the metal atoms. For instance, there is a weak threshold at 21.8 eV for O^+ desorption from TiO_2 due to an intra-atomic transition to the O 2p level, which leaves limited energy available for desorption. However, a strong threshold exists at 34 eV corresponding to an inter-atomic Ti 3p hole decay.[24] O^+ desorption is less likely from materials with valence electrons left on the metal atoms, as in NiO and Cr_2O_3 found on stainless steel surfaces. In these cases, the metal atom core hole can be filled from within the metal atom itself.

An intra-atomic transition can be favored for some species. For example, F^+ and OH^+ have strong thresholds corresponding to the F (31 eV) and O (21.8 eV) core level energies when bonded to TiO_2 because they exist in a -1, not a -2, charge state. Thus, more energy is available from an intra-atomic transition.[24]

There is other evidence of the KF mechanism. F^{2+} ions desorbed from a sputtered aluminum surface had twice the energy of F^+ ions, as would be expected from the Coulombic ejection of the KF mechanism.[25] Also, photon stimulated desorption of H^+, OH^+ and F^+ from TiO_2 verify the KF mechanism since appearance thresholds correspond to core level energies.[26] This photodesorption effect also occurs in semiconductors (CrO_2 in stainless steel). A hole-electron pair is created by

an incident photon and then the hole recombines with the bonding electron, releasing the adsorbed atom.[5,27]*

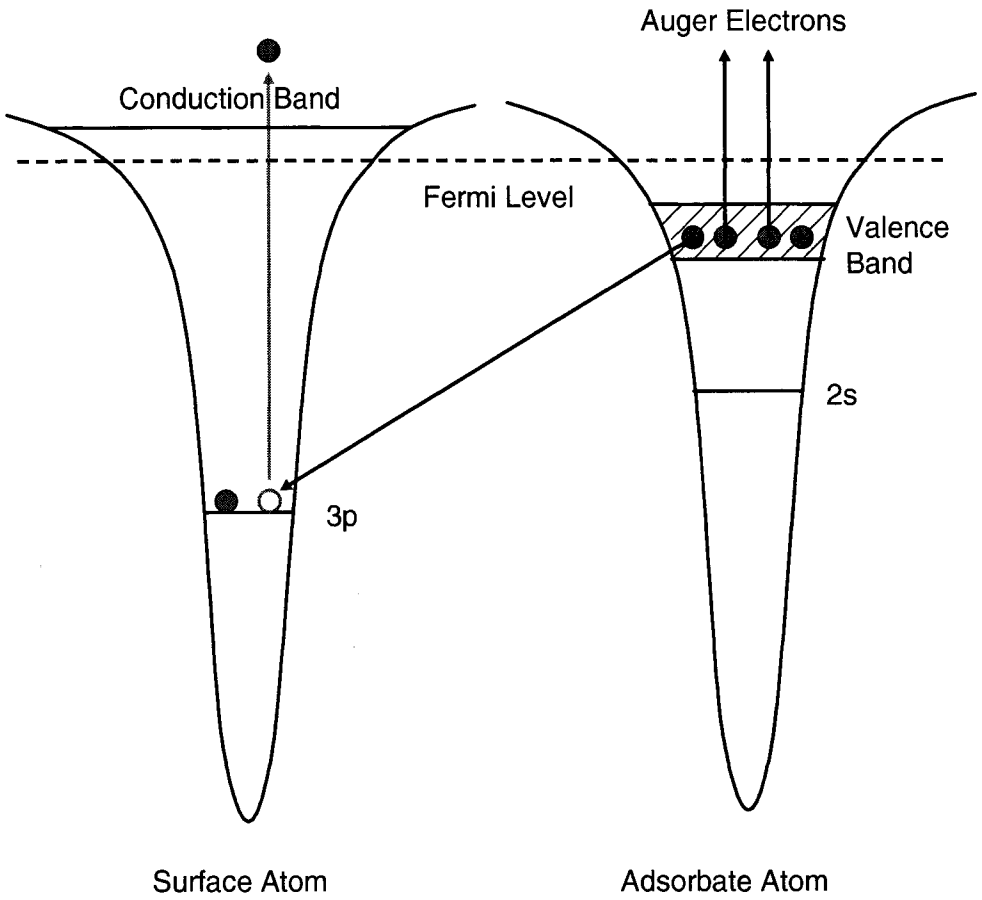

FIGURE 2.2 A schematic of the Knotek-Feibelman model shows an inter-atomic Auger transition after a core hole is formed in the surface atom 3p orbital. The adsorbate is left in a positive state, repulsive to the surface atom.

ESD can lead to errors in total pressure measurements. An increase in local pressure around an ionization gauge due to desorbed neutrals can lead to increased gas phase ionization or additional ESD ions striking the collector of a gauge can give higher pressure indications.

---

* O'Hanlon, p.67

Several methods have been suggested in order to reduce the error (sometimes a factor of 10 to 100) associated with ESD in measuring system pressure. The modulated Bayard-Alpert gauge design adds a modulation electrode to the conventional geometry to differentiate gas phase ions from surface ions and x-ray generated photoelectrons. The extractor ion gauge has its collector out of sight of the grid, so that ESD ions do not reach it directly. Because ions originating from the surface due to ESD have more kinetic energy (several eV) than ions originating in the gas phase from electron impact, they collide with the shield instead of being reflected toward the collector.[28]* Grid heating techniques have been also been suggested.[29] Heating a Pt grid to approximately 500 °C after previous cleaning by electron bombardment to 1000 °C seems to minimize the spurious H peak from out-diffusion and subsequent stimulated desorption.

ESD also causes errors in partial pressure measurement and analysis.[6] Anomalous peaks in double-focusing mass spectrometers (e.g. QMS or E × B) can be seen, as ESD surface ions are detected. If not understood, they may be incorrectly identified.

2.2.1 Bonding states and surface reactions

The results of electron bombardment of adsorbed surfaces are dependent on the bonding states of adsorbed species, what species coexist on the surface, the surface material and the surface condition (defects). The bond location and

* Ellefson, p.421-422

orientation when a molecule adsorbs may determine whether it desorbs through a first or second order process. Both adsorption and desorption can be affected by surface condition, since defects can provide reaction sites. The presence of surface contaminants and multiple adsorbates may lead to electron stimulated reactions.

A good example of the effects of bonding states is the case of carbon monoxide on metals.[20] CO adsorbs on tungsten in several possible states. One orientation (β-CO) has both atoms bound to the surface and thereby weakening the C-O bond. Another more weakly bound orientation is where the carbon atom is attached to the surface by a single bond (α-CO). The molecule can also be double bonded between the carbon atom and the surface. The double bonded carbon state will tend to leave a carbon residue and can be converted to the β-CO state upon electron bombardment. These states may have sub-states that yield either CO^+ or O^+ by ESD. The tendency seems to be that CO initially adsorbs in the strongly bound state with lower ESD cross-section, with subsequent adsorption on neighboring sites having weaker bonding. This is consistent with the fact that electron stimulated desorption of CO^+ from CO adsorbed on W decays rapidly with time compared to O^+ desorption rate decay.[20]

As another example, at low temperatures (< 100 K) nitrogen adsorbs on tungsten in two groups of states: strongly bound atomic states and weakly bound molecular states. The atomic states do not seem to be influenced by electron bombardment.[20] The molecular nitrogen can be converted to an excited molecule by electron bombardment and can subsequently be converted to an atomic species.[20]

The substrate material can determine the bonding state of the adsorbed species. For instance, CO seems to adsorb molecularly on Ruthenium (001), with the C-O bond angled from the surface.[30] However, CO adsorbs dissociatively on stainless steel and desorbs through second order recombination processes as determined by temperature desorption spectroscopy and Auger electron spectroscopy.[31,32]

Electron stimulated reactions are also possible on surfaces and depend on surface conditions and the types of adsorbed atoms and molecules. For instance, hydrogen and oxygen can react with carbon to produce methane and carbon monoxide.[5]* Photo-dissociation of adsorbed O_2 with the O-O bond parallel to step-edge sites on Pt will tend to eject an O atom toward a CO molecule producing CO_2 that desorbs.[33] Similar orientation specific reactions could also take place between other constituents during electron bombardment, like water and hydroxyls.

2.2.2 Fluorine

The prevailing thoughts about the source of ESD fluorine are that the fluorine either exists in the grid of ion sources and gauges *a priori* or through some processing step. Another thought is that it is transferred to the grid in some manner, such as from heated filaments,[34] migration of alkali halides[14] or accretion from the background.[35] Certainly where fluorine-containing compounds are used (e.g.

* O'Hanlon, p.66

CCl_2F_2), ESD fluorine can be expected.[36,37] Nevertheless, F^+ generation is unlikely compared to F^- generation for such electronegative compounds.

Experiments by de Moraes and Lichtman[38] using a magnetic sector mass spectrometer show that with increasing coverage of CCl_2F_2 on a clean W surface, yield at 19 amu (attributed to F^+) increased, flattening to a near constant current at about 5 Langmuir. Desorption was observed with a coverage as low as 10^{-4} Langmuir. The decay in signal during ESD was found to follow the sum of two exponentials with cross sections found to be 4.5×10^{-18} cm^2 and 5.4×10^{-19} cm^2. The coverage sensitivity of ESD to fluorine from CCl_2F_2 on W is estimated to be 3×10^9 atoms/cm^2 whereas sensitivities of AES and XPS are on the order of 10^{11} or 10^{12} atoms/cm^2. The ESD sensitivity to F was 10 times greater than that for Cl.[38] In contrast to CCl_2F_2, the F ion current from C_2F_6 on W decayed more rapidly, again as the sum of two exponentials, with cross sections of 1×10^{-17} and 9×10^{-19} cm^2.[37]

Park *et al.*[39] coated a W(100) surface with the fluoride flux from a CoF_3 oven. The W crystal could be heated and bombarded with an Auger electron gun. The ion energy distribution was measured using a cylindrical mirror analyzer and showed the onset of desorption at 15 eV with peaks at 27, 36, 47 eV. The 36 and 47 eV peaks correlate well with ionization potentials for W core levels, suggesting the KF mechanism involving inter-atomic Auger decay, described in section 2.2. However, it is not likely that fluorine removes enough valence electrons from W to induce an inter-atomic Auger decay, so this disagrees with the maximum valency argument of KF.

The 27eV peak is likely due to the fluorine 2s core level at 31 eV with correction for the surface work function.[39] This agrees with other work where fluorine can be removed from a CaF_2 surface via ESD if the electron energy is above 28eV. Both cases point to the intra-atomic Knotek-Feibelman mechanism.[40]

The 15 eV threshold, however, is explained best by the MGR mechanism, described in section 2.2, where the energy necessary to excite and desorb an atom is given by $(E + \varphi)$, such that

$$(E + \varphi) = V_i - \varphi + E_k + E_d \qquad (2.8)$$

If the adsorbate is considered near the vacuum level, the energy available for the process is $(E + \varphi) - \varphi$, and, thus,

$$E = V_i + E_d + E_k - \varphi \qquad (2.9)$$

where E is the kinetic energy of the incident electron, E_k is the kinetic energy of the desorbed atom, V_i is the ionization potential of the adsorbate, E_d is the desorption activation energy, and φ is the work function of the substrate.[39]

As the substrate temperature was raised, the desorption current dropped. This cannot be explained by the MGR model because the current would increase due to increased distance between adsorbed species and the surface. However, increased fluorine-tungsten distance would decrease inter-atomic Auger decay, as explained by the KF mechanism. Flashing the W crystal to 2000 °C eliminated the ESD signal and

there was no increase after 2 hours. This suggests that the F^+ ion signal was not attributable to residual gas adsorption or diffusion of F from the bulk to the surface. The persistence of the F^+ signal after heating the W crystal to 1500 K at low coverage suggests dissociative adsorption of fluorine because it is tightly bound.[39] Work with SF_6 is also best explained by dissociative adsorption.[41]

Different substrates can lead to slight differences in the desorption mechanism. Fluorine adsorbs as F^- ions on aluminum and is strongly bound. F^+ ions are found bound to aluminum but their adsorption energies are lower and their equilibrium distance is further from the surface. The difference in bonding is due to different screening mechanisms. Negative ions are screened only by an image mechanism, where the surface acquires a balancing positive charge. Positive ions are screened by both image and charge-transfer mechanisms, where electrons from the metal substrate can occupy large radius 3s and 3p orbitals.[42]

For desorption of fluorine from silicon, two mechanisms can occur.[43,44] If a F anion core hole is first produced, an intra-atomic Auger decay can fill the F core hole, and the atom is left in a +1 charge state. This leads to Coulomb repulsion between the nascent F^+ ion and Si cation. If a Si cation core hole is produced first, an inter-atomic Auger decay is necessary to form F^+ and tends to occur because so much charge is transferred to the fluorine in forming the chemical bond. For chlorine adsorption, this process is quenched due to less original charge transfer.[43,44]

From the experiments above, the ESD behavior of fluorine tends to agree more with the KF mechanism, but may not always agree with the maximum-valence argument. The specific process can also be influenced by the type of substrate. In

cases where fluorine-containing compounds are under study, fluorine is a more probable explanation for a signal at mass 19.

Over the years, however, there have been a number of experiments where the signal at mass 19 was attributed to fluorine, but may have actually been hydronium because there was no obvious source of fluorine. In an experiment by Floyd and Prince,[35] the fluorine source was supposedly an hour of background accretion after tungsten was heated to 2200 K. Two total desorption cross-sections were found for F^+ (or perhaps H_3O^+) on W: 2×10^{-18} and 3×10^{-19} cm^2, and the ionic desorption cross-section of one possible state was 3×10^{-20} cm^2. [35]

In another experiment on tungsten by Yates and King,[34] the mass 19 signal increased each time the ThO_2 coated W filament was taken to a higher temperature with no respect for biasing, indicating a neutral fluorine-containing species is transferred. Suggested species were WOF_4 and $ThOF_2$. Repeated heating of the sample to 2500 K reduced the signal.[34] However, hydrogen and oxygen are more likely to have been transferred.

Other work with stainless steel has yielded a fluorine (perhaps H_3O^+) ESD cross-section at 1000 eV of 9.6×10^{-18} cm^2. Heating the target to 450 °C and allowing the target to equilibrate for several hours without heat or bombardment, supposedly hastened fluorine buildup, but it also increased the partial pressures of water and H_2. Upon electron bombardment, the fluorine signal was also noted to increase initially. This was suggested to be due to H being freed from surface sites that were then occupied by F. But it could also be due to a flash of water vapor or H_2.[12]

It is normally suggested that fluorine desorbs via the KF mechanism. However, experiments have shown that the threshold for F^+ emission (perhaps H_3O) from W (100) was approximately 24 eV and does not occur near the F 2s binding energy of 31 eV (also listed at 37.2 eV) or any W levels as the KF mechanism would require. The threshold for Cl^+ was at 17 eV, corresponding well with the Cl 3s level and supporting the KF intra-atomic Auger mechanism.[45] The threshold correlates better for hydronium since the O 2s binding energy is at 28.7 eV. The difference could then be due to energy required to break the metal-O bond and other H bonds. Fluorine binding energy is reportedly above 3 eV on W[35] and 4.65 eV on Mo.[46]

2.2.3 Precursors of water and hydronium

It is helpful to understand how oxygen, hydrogen and hydroxides behave when bombarded with electrons, since they are the precursors of water and hydronium. Fortunately, there has been a considerable amount of work exploring ESD of these species.

Oxygen is almost always found at the surface of metal substrates in an oxide layer. It will sometimes be removed preferentially by electrons interacting with metal oxides, and Auger studies have shown the decrease in oxygen signal and the chemical shift of metal atoms from oxide to metallic states. This has been seen with oxides of several metals, such as aluminum, molybdenum, tungsten and niobium.[21]

The oxygen on tungsten system is complex. Under electron bombardment there is evidence of two adsorbed states, one that does not yield a significant number

of ESD O^+ ions (cross section $< 2 \times 10^{-23}$ cm^2) and one that did with a cross section of about 3×10^{-20} cm^2. The ion yield state is molecular and makes up only a small fraction of the total surface coverage.[20] Oxygen on W (100) seems to desorb according to the KF inter-atomic Auger mechanism since the thresholds seen correspond to W core-levels. The threshold was found to be about 24 eV.[45]

Hydrogen is the most prevalent element in the universe and, because it is so small, it permeates almost every material. In vacuum systems, it is found throughout the bulk of metal chamber walls and in the substrates of samples being tested. Because it is so pervasive, it is the main constituent of the residual gas atmosphere in most ultrahigh vacuum systems.

Using ESD mass spectrometry, it has been shown that H_2 initially adsorbs on Ni molecularly and yields ESD H^+. Upon heating, there is a conversion to a more strongly bound atomic state and the H^+ signal is cut in half. Heating to 730 K leads to H_2 desorption and the H^+ signal disappears.[20]

ESD H^+ ions leave surfaces with some kinetic energy which may differ depending on substrate and source. Molecular hydrogen is an obvious source of H^+. Water can be a source of ESD hydrogen ions as well, but is not usually a source of molecular H_2^+ ions. The H^+ mass 1 peak tends to follow water vapor partial pressure.[10] H^+ ion emission energy was found to be near 2 eV from H_2 on W and near 4 eV for H_2O on W.[47] Additional ion energy distribution data for surface species (most likely water) from tungsten show maxima at 4.4 eV for H^+, 4.5 eV for F^+ (perhaps H_3O^+) and 10.2 eV for O^+.[9]

Other results on stainless steel show the ESD ion energy to peak at 3.3 eV for H^+ and 2.3 eV for F^+ (perhaps H_3O^+). The H^+ ESD cross-section at 1000 eV was found to be 1.3×10^{-16} cm^2. When the SS is taken above 450 °C for several hours, the H^+ signal decreases to zero while F^+ (H_3O^+) stays fairly strong. Upon cooling, the F^+ is still strong and the H^+ signal returns to original levels.[12]

2.2.4 ESD of water and hydronium

There has been considerable interest in electron and photon stimulated desorption of water, especially in the area of astrophysics. Electron and photon dose and substrate temperature have a great effect on yields, which suggests a second order process involving precursors.[17,48] On metal surfaces, the strong chemical interaction with water limits the lifetime of electronic excitations of adsorbates, while on weakly physisorbed surfaces the excitation lifetime is longer since the excitation is confined to the overlayer. This allows other channels for water desorption or dissociation.[17]

When D_2O was adsorbed on a solid Ar substrate the ESD yield of D_3O^+ and other $D^+(D_2O)_n$ cluster ions was highest at low exposure (< 1 monolayer) and decreased with increasing coverage. However, the D^+ yield was found to increase with increasing coverage. The D^+ ion desorption results from dissociative ionization of D_2O and the D^+ yield is related to the number of O-D bonds at the top surface layer. The cluster ions are ejected by Coulombic repulsion from valence holes created by Auger decay. In order for this to occur, the holes need to be confined in the cluster

for more than 10 fs without diffusing into the substrate. On metal substrates, the chemical interaction with water can delocalize valence holes, leading to few desorbed positive ions other than H^+.[17]

Valence holes are absorbed by the hydrogen in water forming protons which are then available to form hydronium ions. Proton diffusion occurs on the order of 1 ps, much longer than the time needed for Coulombic repulsion or the diffusion of valence holes (1 fs).[17] Thicker layers of water tend to delocalize the valence holes due to the hydrogen bonding network. Because of hydrogen bonding, the cohesive energy of water (6.1 kcal/mol) is much larger that of the argon substrate (1.85 kcal/mol).[17]

An alternative mechanism of hydronium desorption is supported by ultraviolet photon stimulated desorption in a water-on-graphite system. Again higher water coverage leads to lower yields of H_3O^+ (D_3O^+), while H^+ (D^+) increased with increasing coverage. This is most likely because fewer hydrogen bonds must be broken in low coordination sites. Also, sufficient photon energy is required for desorption to occur. With 21eV photons, only H^+ (D^+) desorbs, while with 41eV photons, hydronium is also desorbed. The D_3O^+ signal was greater than D^+, whereas the H^+ signal was greater than H_3O^+, suggesting that D^+ transfers momentum to a D_2O molecule more efficiently than H^+ to H_2O. [48]

The proposed mechanism for H_3O^+ desorption requires a dissociative photo-ionization event that breaks the O-H bond in a water molecule that is in close proximity to another low coordination number water molecule (i.e. near the surface). Since the water molecules are hydrogen bonded, the free proton will move along the

axis of the bond and combine with the other water molecule to form H_3O^+. The proton provides sufficient kinetic energy to the hydronium to break the other hydrogen bonds (~ 0.25 eV each) and overcome the image charge attraction (~ 0.6 eV). H is not as massive as D, hence less momentum is available and the yield of H_3O^+ is smaller than that of D_3O^+. There seems to be a preferential breaking of hydrogen bonded O-H bonds over free O-H bonds. This could be due to the fact that the reaction to form D_3O^+ is more exothermic (7.3 eV) than that to form D^+ or perhaps more modes of vibration absorb additional energy.[48]

2.3 Stainless Steel and Chromium Oxide

The 300 series of austenitic stainless steels, characterized by an iron-carbon alloy containing more than 13% chromium, is the most frequently used in gas handling instrumentation and vacuum systems; 304 and 316 are the most common.[5] Austenitic stainless steel has a face-centered cubic (fcc) structure at room temperature because it is stabilized by the alloy addition of nickel. For example, the composition (wt. %) of 316 stainless steel is C (0.08), Mn (2.0), Si (1.0), Cr (16 to 18), Ni (10 to 14) and Mo (2 to 3).[49] The 300 series stainless steel is used in vacuum systems because it is resistant to corrosion, easy to weld and is non-magnetic. It can also have a low outgassing rate because of the oxide layer that can form on the surface.[5]*

The presence of chromium is what gives the steel its corrosion resistance and low outgassing rate. Chromium diffuses to the surface of the steel and forms a very

* O'Hanlon, p. 289

stable oxide, Cr_2O_3. The sizes of chromium atoms and their oxides are similar, so they form a stable oxide that can be several atomic layers thick with a high packing factor due to the similar atom ratio of Cr and O. Cr_2O_3 has the corundum crystal structure and a rhombohedral Bravais lattice that closely approximates a hexagonal lattice having close packed O^{2-} sheets with 2/3 of the octahedral interstices filled. There are 30 ions per unit cell: 12 Cr^{3+} and 18 O^{2-}. [49] A representation of the structure of Cr_2O_3 is shown in Figure 2.3.

If the stainless steel is heated to high enough temperatures (~ 800°C), more chromium will segregate to the surface and scavenge oxygen from the iron, forming a thicker oxide layer. If raised to higher temperatures, the chromium can evaporate out of the steel. In fact, during welding of stainless steel parts, the chromium can be depleted in regions adjacent to the weld leaving those areas susceptible to corrosion.[49]

If the metal is cut or scratched and the passive film is disrupted, more oxide will quickly form and recover the exposed surface, protecting it from oxidative corrosion. (Iron, on the other hand, rusts quickly because atomic iron is much smaller than its oxide, so the oxide forms a loose rather than tightly-packed layer and flakes away.) The passive film requires oxygen to self-repair, so stainless steels have poor corrosion resistance in low-oxygen and poor circulation environments. In seawater, chlorides from the salt will attack and destroy the passive film more quickly than it can be repaired in a low oxygen environment.[50]

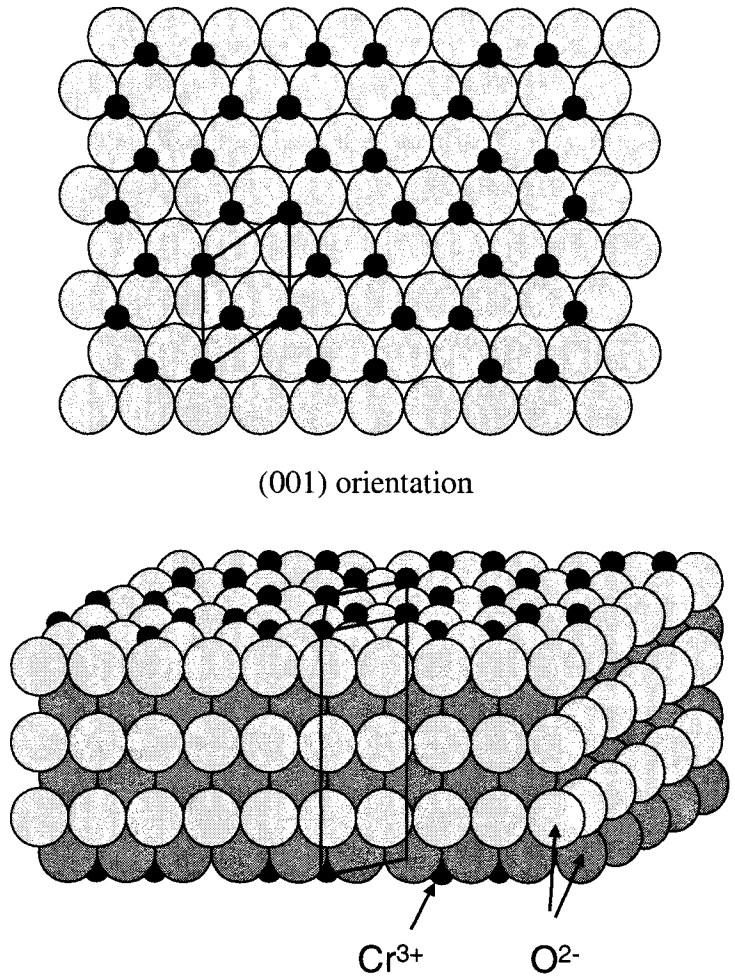

FIGURE 2.3 Cr_2O_3 has the corundum structure. The unit cell is shown superimposed on both top and side views. Black dots are Cr^{3+} ions. The chromic oxide serves as a capping layer for the bulk stainless steel.

Carbide precipitation and inclusions can also be problems when using stainless steel for vacuum vessel fabrication. The carbon that precipitates at grain boundaries during welding or improper cooling can deplete chrome from surrounding areas, causing them to be susceptible to corrosion. One solution to this problem is to use a low carbon steel alloy, such as 304L or 316L.[5]*

* O'Hanlon, p. 305

2.4 Water

Compared to other small molecules, water behaves rather differently. Water has a large heat capacity, a high latent heat of evaporation, and has unusually high melting, boiling and critical points. For instance, methane melts at -182 °C and boils at -164 °C, even though it has a lower molecular weight than water. Water also has unusually high surface tension, viscosity and thermal conductivity. These can all be explained by the formation of hydrogen bonds between the water molecules.

The water molecule is highly polar because the oxygen atom has two lone pairs of electrons that are not involved in a bond. These electrons are situated to one side of the oxygen atom, giving that side a slightly more negative charge. The electrons involved in the bonds with the hydrogen atoms spend more time between the hydrogen and oxygen atoms, exposing the more positive hydrogen nucleus. Therefore, the hydrogen atoms of one molecule can be attracted to the oxygen atom of another, yielding potentially four hydrogen bonds per molecule. These hydrogen bonds require extra energy to break, giving rise to the properties above. Because the hydrogen atoms and electron pairs are situated at close to tetrahedral angles around the oxygen nucleus, liquid water can have a degree of three dimensional structuring and can be thought of as existing in ionic clusters.[51]

The strongest of all the bonds involved with water is the covalent bond (sharing of electrons) between H and O, which has an average energy of 460 kJ/mol (110 kcal/mol or 4.5 eV). The bond between a water molecule and a surface is considered a dative bond (involving electrical attraction) and is on the order of 40 to

90 kJ/mol (10 to 20 kcal/mol or 0.4 to 0.9 eV). Finally, the hydrogen bond (between H of one water molecule and O of another) is typically only about 23 kJ/mol (2 to 10 kcal/mol or 0.08 to 0.4 eV), but is still stronger than van der Waal's bonding, which is typically about 1.3 kJ/mol (0.3 kcal/mol or 0.001 eV).[52] Ionic bonds (electrostatic) are typically between 16 and 30 kJ/mol (4 and 7 kcal/mol or 0.1 to 0.3 eV), but can be much higher. The hydrogen bond is mostly a dipole-dipole bond, but is partly covalent. A range of bond strengths are given in Table 2.1 and some common covalent bond enthalpies are given in Table 2.2.

TABLE 2.1 Bond types and their energies.

	Bond Type	Bond Energy (kJ/mol)
Stronger Primary Bonds	Ionic Bond	16 to 600
	Covalent Bond	150 to 900
	Metallic Bond	140 to 500
Weaker Secondary Bonds	Hydrogen Bond	10 to 40
	van der Waals	0.02 to 40
	Dipole-dipole	0 to 20

TABLE 2.2 Some covalent bonds and their energies.

Bond Type	Average bond enthalpy (kJ/mol)
C–H	+ 413
C–C	+ 347
O=O	+ 498
C=O	+ 805
H–O	+ 464

It is possible that the hydrogen atom involved in a hydrogen bond may spend more time near the other water molecule and actually transfer to become part of that molecule. This results in two ions, the hydroxide ion, OH^-, and the hydronium ion, H_3O^+. This actually occurs frequently, though the ion concentration at any given instant in pure water is small, only 10^{-7} moles/L. The tendency for a water molecule to accept another hydrogen atom, or more correctly, another proton, is given by its proton affinity of 690 kJ/mol (165.2 kcal/mol or 7 eV). Proton affinities of some common gaseous molecules are given in Table 2.3.

TABLE 2.3: Proton affinities for various molecules.[53]

Molecule	Proton Affinity kcal/mol
H_2	100.9
N_2	118.0
CO	141.7
H_2O	165.2
CH_3OH	180.3
C_2H_5OH	185.6
NH_3	204.1

NIST Standard Reference Database Number 69 – August 1997 Release

2.5 Water – Surface Interactions

The water-metal and water-oxide surface interaction is important in many scientific and technological areas, especially in vacuum science, but is not well understood. Water can adsorb intact on the surface of inert transition metal surfaces with high coordination number, forming a buckled hexagonal ice bi-layer,[54] and

will desorb mostly intact from metals like Ru, Rh and Pt.[55] However, calculations show that partial dissociation should occur on the surface of Ru (0001), forming an overlayer of OH and H_2O.[56]

How water molecules bind to uncharged metal surfaces depends on the nature of the metal and on co-adsorbed species. On a platinum Pt(111) surface half of the water molecules bond by way of the oxygen atom to form Pt····OH_2 links.[57] The other half form Pt····H-OH bonds as Pt····H bonds form and H-O bonds weaken. Other metal surfaces may prefer a particular water orientation or cause partial dissociation of the protons dependent on their proton affinity.[57] It has also been proposed that when O is adsorbed with H_2O on Pt (111) a mixed OH/H_2O over-layer forms which then orders to become a stable (3×3)- 3(OH + H_2O) phase.[54]

When metal surfaces are biased, even with low voltages, the orientation of the water molecules and the positioning of ions can be significantly affected.[58] A negative potential of will orient water hydrogen atoms towards the electrode whereas a positive potential reverses the configuration. This orienting can cause some hydrogen bond breakage and a local increase in water density.

Since ions are attracted or repelled depending on their charge, similar orientations may occur at the surface of non-metals with alternating positive and negative charges. A solid (static and non-exchangeable) water layer has been reported to form at the surface of metal oxides that are highly polar *(e.g.* TiO_2) and modeling reveals that, through a process called ice tessellation, a single monolayer of ice may form on the surface of hydrophilic fully hydroxylated silica. This may explain why layers of structured water are found at the surfaces of complex silicates.[59]

On well ordered Cr_2O_3 (0001) surfaces, water adsorbs almost entirely as a molecule at lower temperatures with dissociation taking place near oxygen defect positions.[60] In the case of stainless steel, the surface is polycrystalline and full of defects. The passive chromium oxide film on the surface of stainless steel may be more accurately thought of as a chromium enriched oxide in a hydrated gel structure. The overall CrO_x film is around 2 to 4 nm thick.[61]

2.6 Generation of Moisture in Vacuum

In spite of the passive nature of stainless steel, there is evidence that the surface is not necessarily inert. Research has shown that water can be formed when the steel is exposed to a hydrogen atmosphere.[62] The amount of water formation depends linearly on the amount of hydrogen present and the temperature of the surface. If the surface is heated to 900 °C in an oxygen atmosphere, its ability to produce water is reduced. Apparently, the source of oxygen is surface oxides, carbon oxides or oxygen diffusing from the bulk. In the case of surface oxides, Cr_2O_3 is so stable that it is seen as a less likely candidate for the source of water than iron oxides or nickel oxides. The enthalpy of reaction at 400 °C for reduction of NiO to Ni is - 8 kJ/mol-H_2O, compared to 34 kJ/mol-H_2O for Fe_3O_4 to Fe and 102 kJ/mol-H_2O for Cr_2O_3 to Cr.[63] Thus, other constituents of stainless steel could contribute to moisture formation. Since heating brings more chromium to the surface of stainless steel, the evidence of reduced water formation supports this hypothesis.[62]

Other metal surfaces may have the capability of generating water from constituent elements as well. Co-adsorption of hydrogen with oxygen on palladium can have various structures depending on the surface temperature because structural changes occur as hydrogen diffuses in and out of the bulk. Above 220 K oxygen is lost from the Pd surface due to formation of OH and subsequently H_2O as hydrogen segregates from the bulk.[64]

2.7 Hydroxides on Chromium and Stainless Steel

It is generally accepted that the passive film that forms on the surface of austenitic stainless steels consists of an inner and outer layer, as shown in Figure 2.4. The outer hydroxylated layer (~ 15 A) is mostly chromium hydroxide containing some iron hydroxide, while the inner oxide layer (20 – 40 A) is chromium oxide with some iron oxide, chromium and iron. XPS and TOF-SIMS data support this conclusion, with TOF-SIMS unambiguously showing the presence of positive and negative ions of CrOH and FeOH.[18,65] A sub-layer is found below these layers containing chromium, iron and nickel oxides with chromium, iron and nickel metal. Alloys with higher chromium content seem to have a thinner chromium oxide layer, but are more corrosion resistant. This is possibly because oxygen reacts with the chromium mostly on the surface leading to a dense film that retards inward diffusion of oxygen.[65]

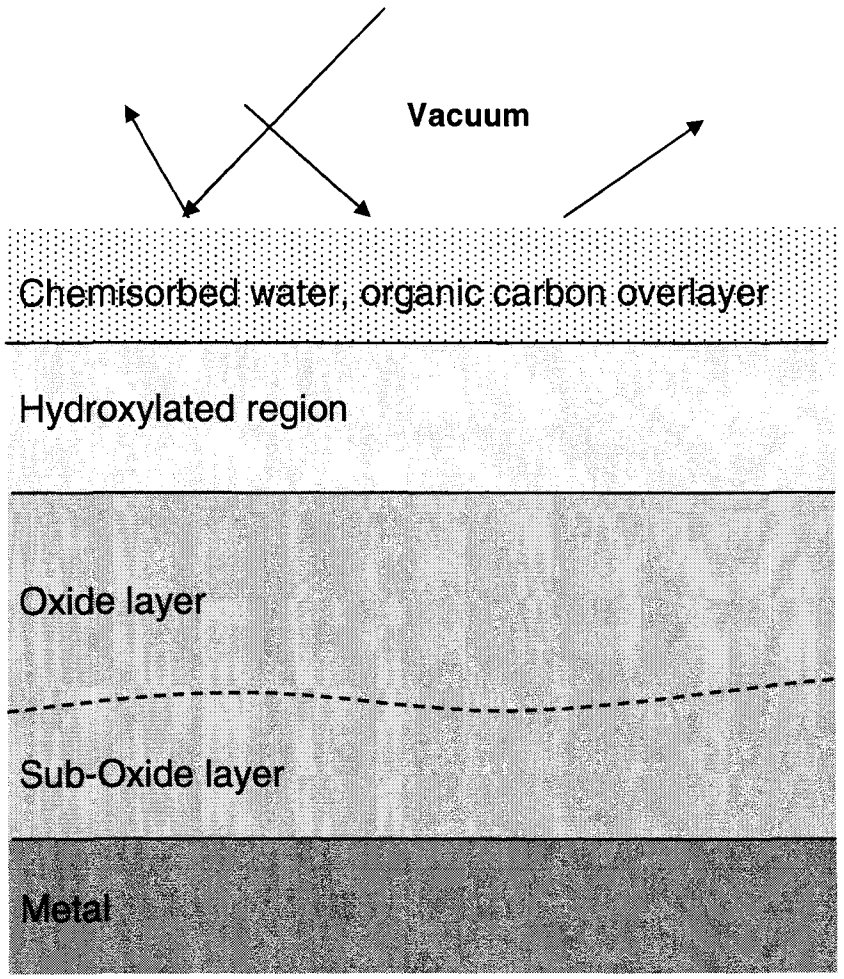

Figure 2.4 A general schematic of the stainless steel surface.

Exposure of Cr_2O_3 to water vapor has been shown to result in hydroxylation of the surface due to water dissociation.[66] X-ray photoelectron spectroscopy (XPS) shows a higher binding energy shoulder near 531.4 eV on the O 1s peak at 530.7 to 530.9 eV. The Cr $2p_{3/2}$ region shows three features corresponding to chromium (B.E. = 574.4 eV), chromium anhydrous oxide (B.E. = 576.5 to 576.7 eV) and chromium hydroxide (B.E. = 577.2 to 577.4 eV).[66] Data from stainless steel often show the O 1s peak closer to 530.0 eV.[18,65] Scanning tunneling microscopy (STM) data show

that the hydroxylation reaction is not specific to defect sites, however it does lead to a disordered and corrugated surface, suggesting OH induced surface diffusion and rearrangement. Low energy electron diffraction (LEED) data show that the bulk oxide lattice is not modified.[66]

Water can adsorb on Cr_2O_3 in the molecular state and in dissociative stages. The molecular state desorbs at 295 K and the dissociated state desorbs at 345 K.[67] High resolution electron energy loss spectroscopy (HREELS) reveals an isolated terminal O-H bond and a bridging O-H bond involved in an unusually strong hydrogen bond with the other oxygen. The Cr^{3+} cation involved with the terminal O-H group can also bind another non-dissociated molecule of water.[67]

The abundance of hydroxides on the surface of stainless steel makes hydronium a more likely source of mass 19 than fluorine. Several sources have shown that the XPS signals from oxides and hydroxides can be deconvoluted and that the effects of various processes, such as heating and hydration, can change these signals.[18,65-69]

2.8 Hydronium

As is indicated by the "unusually strong" hydrogen bond in the section above, it stands to reason that the surfaces of metals and metal oxides are a matrix for the formation of hydronium. HREELS (High Resolution Electron Energy Loss Spectroscopy) and ATR-FTIR (Attenuated Total Reflection Fourier Transform

Infrared Spectroscopy) have indicated the existence of hydronium ions on the surface of single crystal platinum, silicon and germanium.[70,71]

In the case of platinum surfaces, it is suggested that a lone hydronium ion does not form, but larger clusters instead, such as $H_7O_3^+$. The enthalpies of reaction favor the larger clusters. $H(ad) + H_2O(ad) \rightarrow H_3O^+(ad) + e^-(ad)$ has an enthalpy of 130.5 kJ/mol (31.2 kcal/mol), whereas $H(ad) + 3H_2O(ad) \rightarrow H_7O_3^+(ad) + e^-(ad)$ has an enthalpy of 33.6 kJ/mol (8.04 kcal/mol). For $H_9O_3^+$ it is -4.4 kJ/mol (-1.06 kcal/mol).[72]

From the research presented in this chapter, we see that the surfaces of materials, stainless steel and Cr_2O_3 in particular, can be quite chemically active. The interaction of water and hydrogen with surface oxides to form hydroxides and hydronium is very pertinent. We have learned about electron stimulated desorption and we can surmise that ESD of hydronium from stainless steel, even when no water is introduced into the vacuum system, is certainly plausible. Next we experimentally determine the nature of the mass 19 peak in spectrometers and explore the effects of electron bombardment on stainless steel and chromium oxide.

CHAPTER III

EXPERIMENTAL

In the previous chapter, we learned about how atoms and molecules can adsorb and desorb from surfaces, particularly through electron stimulated desorption (ESD). We understand that this process can lead to anomalous peaks in mass spectra. Additionally, hydronium was seen to form on surfaces. Now we explore the behavior of mass 19 in mass spectrometers and how this behavior may correlate to hydronium.

3.1 Fourier Transform Mass Spectrometry

An ion cyclotron resonance (ICR) Fourier transform mass spectrometer (FTMS) was used to resolve the contributors to the signal in mass spectra at 19 amu, in order to show that hydronium is a possible source. The resolution of the instrument was demonstrated, showing the actual composition of several peaks containing species close in mass number. Fluorine and hydronium were resolved and the effects of water concentration on hydronium formation were explored.[3]

3.1.1 Theory and Operation

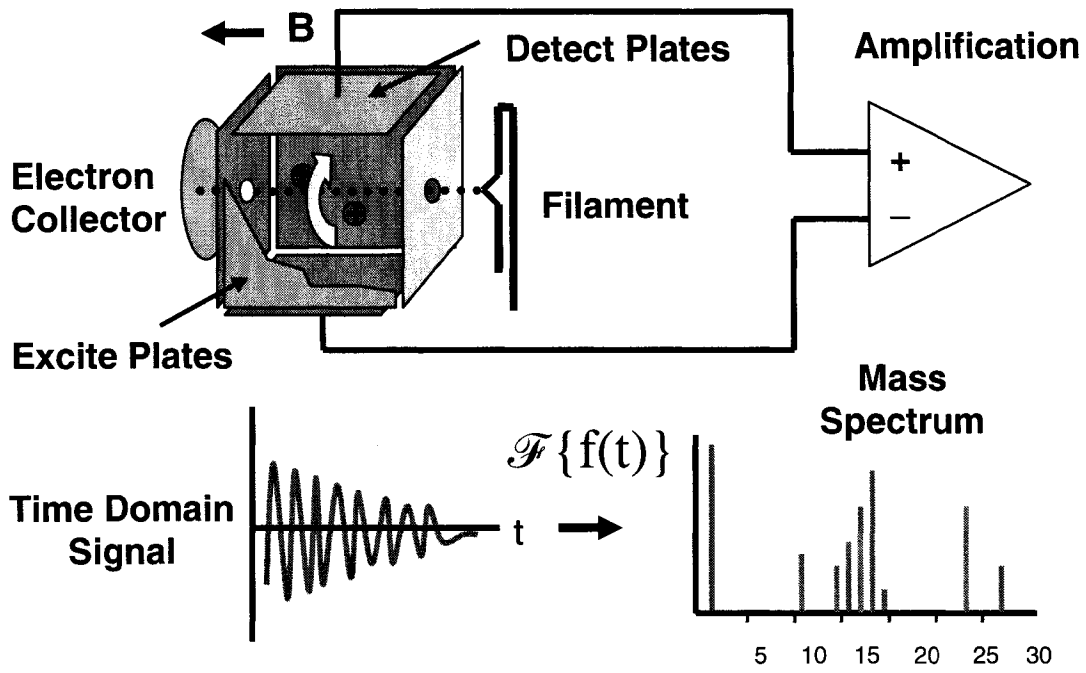

FIGURE 3.1 A schematic of an Ion Cyclotron Resonance Fourier Transform Mass Spectrometer.

An FTMS instrument normally requires a great deal of electronic circuitry and control software for operation. A simplified schematic of the instrument is shown in Figure 3.1. Electrons emitted from a hot filament cathode are pulsed through a cylindrical or cubic ion trap. The current is normally varied between 1uA at lower pressures ($< 10^{-8}$ Torr) and 100 nA at higher pressures ($> 10^{-7}$ Torr) to achieve proper signal strength but avoid space-charge effects. Ions are formed by electron impact ionization within the trap. A highly uniform, axially parallel magnetic field (typically > 1 Tesla) keeps both the electron beam and resulting ions confined to the axis of the cell. The ends of the cell are biased to trap the ions when the beam is off. A small

amplitude (1 to 2 V) radio frequency chirp (a few kHz to a few MHz and pulse width of a few msec) is then applied to the sides of the cell perpendicular to the beam axis. This causes all the ions to go into circular motion around the magnetic field lines.[3] The rotation frequency (cyclotron frequency) depends on the mass of the ion. After the excitation, the motion of the ions induces an image current in the sides of the cell that fluctuates at the ion cyclotron frequencies generated. The cyclotron frequency is given by

$$f_c = \frac{qB}{2\pi m} \qquad (3.1)$$

where q is the ion charge, B is the magnetic field strength and m is the ion mass. At thermal velocities, these orbits are small (typically, 100 μm), but the chirp applied to the sides of the cell imparts equal energy at all frequencies of interest. This excites the ions to resonance and increases the orbital diameter to near cell size, where they create image charges in the detection plates. The various frequencies are detected simultaneously and are differentiated by Fourier transformation of the time domain signal. Ions in a particular mass range can be ejected by applying a large amplitude preliminary frequency chirp over the corresponding frequencies. This causes them to attain an orbit in which they collide with the cell walls and are neutralized. Ions of interest remain in the cell for analysis. The frequency spectrum is easily converted to a mass spectrum by calibration using the ion cyclotron frequency equation (equation 3.1).[73] Since the mass is inversely proportional to the frequency, the signals get

closer together and the resolving power decreases as the mass increases.[74] Resolving power is given by the equation

$$\frac{m}{\Delta m} = \frac{(0.132)qBT}{m} \qquad (3.2)$$

where m is the mass, Δm is the full width at half maximum of the spectral peak, q is elementary charge, B is the magnetic field strength and T is the acquisition time.

3.2 Quadrupole Mass Spectrometry

Quadrupole mass spectrometry (QMS) has become the most widely used residual gas analysis method in vacuum science and technology. The reasons for the popularity of QMS instruments are rapid mass scanning capability, relatively low cost, compact size, lack of a magnet and linear mass scale. This popularity and the prevalent mass 19 signal that is seen using a QMS prompted its use here. By varying the QMS instrument parameters and operating conditions we can learn more about mass 19.

3.2.1 Theory of operation

In a QMS, ions are usually formed in a hot filament ion source. Electrons from a filament are accelerated toward a cylindrical grid structure. Before they collide with the grid, they make several passes (typically 5 times) in and out of the grid

region where they collide with and ionize gas molecules. The potential between the filament and grid is typically 70 eV because the probability of ionization for most gases is a maximum between 50 and 200 eV.

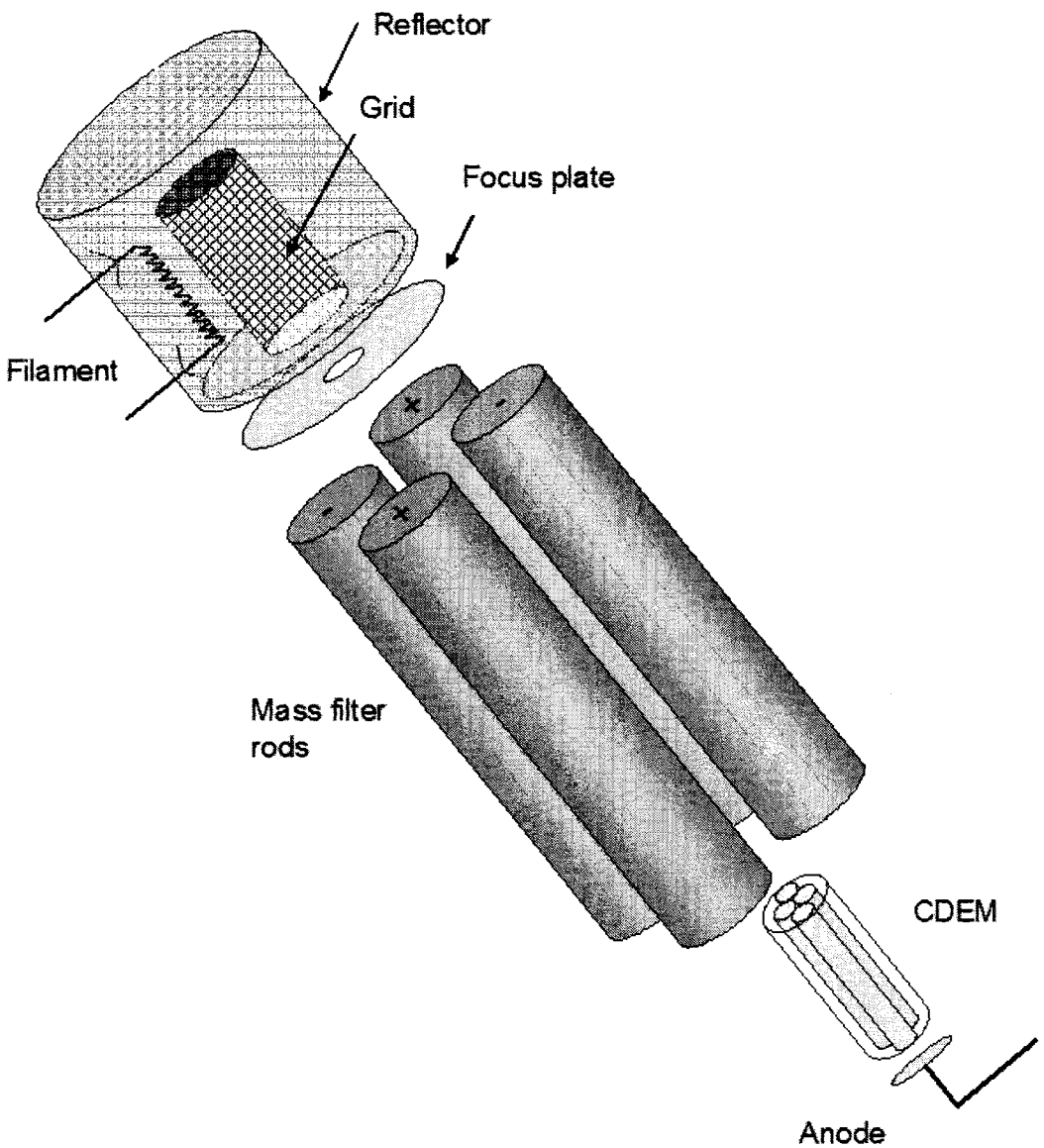

FIGURE 3.2 A schematic representation of a quadrupole mass spectrometer. Ions are formed within the grid of the ionizer, pass through the mass filter rods and strike the continuous dynode electron multiplier (CDEM).

Ions are injected into the quadrupole field formed by four finely machined parallel rods, as shown in Figure 3.2. These rods were originally proposed to be hyperbolic,[75] but circular rods of radius $1.16r_o$ (where r_o is the radius of the circle inscribed by the four rods) work well and are easier to manufacture.[4]*

The rods are energized with a potential given by

$$\Phi = (U - V_o \cos \omega t)(\frac{x^2 - y^2}{r_o^2}) \qquad (3.3)$$

where U is the DC voltage, V_o is the RF voltage, ω is the RF frequency and x and y are the coordinates perpendicular to the axis of the rod assembly. The ion motion is given by the Mathieu equations

$$\frac{md^2x}{dt^2} + \frac{e(U - V_o \cos \omega t)x}{r_o^2} = 0 \qquad (3.4)$$

$$\frac{md^2y}{dt^2} + \frac{e(U - V_o \cos \omega t)y}{r_o^2} = 0 \qquad (3.5)$$

$$\frac{md^2z}{dt^2} = 0 \qquad (3.6)$$

* Ellefson, p. 458

where m is the mass of the ion, e is the charge of the particle and z is the axial position.

Mass separation is accomplished as molecules travel along the changing DC/RF field. Low m/e ions can move almost in phase with the RF voltage and are accelerated to large x and y values until they collide with the rods. High m/z ions are attracted to the negative rods by the DC field where they are neutralized. Between the mass extremes a range of ions can oscillate and drift through the rods without colliding with them and are subsequently detected.

Mass detection is accomplished by measuring the ion current exiting the quadrupole filter using a Faraday cup or an electron multiplier. The Faraday cup is useful when stable signals are required and there is sufficient pressure to generate a detectable ion current using only electronic amplification. The cup retains secondary electrons which would subtract from the detected ion current if lost. Generally, 1×10^{-13} A is the practical detectable limit, corresponding to about 1×10^{-9} Torr.

To measure partial pressures below 10^{-9} Torr, an electron multiplier must be used. There are three main types: discrete dynode, continuous dynode and microchannel plate. In each case, an incoming ion strikes the surface at the front of the multiplier, which has a high secondary electron emission yield, and creates several secondary electrons. These electrons are accelerated to another surface where they each create several more electrons. This cascade continues until a pulse of millions of electrons is detected at the opposite end of the multiplier.

The discrete dynode multiplier has many individual plates that are biased at greater and greater voltage. The continuous dynode multiplier is a long, curved PbO

or Bi_2O_3 tube with a voltage gradient along its length. The microchannel plate multiplier uses many short tubes in parallel.

While usually straightforward, interpretation of QMS spectra can be more subtle than first thought. In addition to ionizing molecules present in the background vacuum, the electron energy in the ionizer is sufficient to dissociate molecules and doubly ionize atoms and molecules. For instance, CO_2 yields a mass signal at 44 amu (CO_2^+), 28 amu (CO^+), 16 amu (O^+), 12 amu (C^+) and 21 amu (CO_2^{++}). Signals that result from ESD ions can further complicate analysis by adding to the expected mass ratios of gases. Resolution and sensitivity can be adjusted by varying the ratio between the voltages U and V_0, but only with a trade-off – as resolution increases, sensitivity decreases and vice versa.

3.3 FTMS/QMS Experimental Approach

3.3.1 FTMS Experiments

Since several mass peaks are often assumed to be a particular atom or molecule, it was interesting to determine the actual composition of the signal at those mass peaks. For instance, mass 15 is normally assumed to be CH_3, a fragment of methane. In order to verify the resolution of the FTMS system, spectra of selected gases with similar mass were obtained, including CO^+ with N_2^+ and O_2^+ with S^+. The N_2^+ and O_2^+ were generated from admission of air, the CO^+ was generated as a fragment of CO_2 and the S^+ was obtained from SF_6.[3]

The resolution of H_3O^+ and F^+ at mass 19 was explored in particular. H_3O^+ was formed from residual water in the FTMS system and F^+ was obtained as a fragment from CF_4. Signal strength dependency on partial pressure was noted.[3] Additionally, parametric studies of signal versus partial pressure of water vapor were conducted. The system was baked to 120 °C for 12h to reduce the pressure, but allowed enough gas phase water to remain for comparison experiments. Heating the vacuum envelope increased the partial pressure of water vapor and this gas phase water was used as the source of H_3O^+ and OH^+.[3]

The typical system pressure was between 1×10^{-8} and 5×10^{-6} Torr, depending on the gas used as a source for the ions of interest. Initially, all ions were purged from the cell by biasing the endplates negatively. This was followed by the ionization period (typically 20 ms) at an emission current of approximately 100 nA. The ions were then trapped in the cell by biasing the endplates at approximately 1.2 V. A frequency chirp was then applied followed by the resonance detection period of approximately 5 ms. These steps were repeated 100 times to improve signal to noise ratio.

3.3.2 FTMS/QMS Experiments

By placing the FTMS near the QMS, the spectra from each instrument could be compared and the contribution at mass 19 was correlated. Then the nature of the mass 19 peak in the QMS was explored by noting its behavior with respect to the partial pressure of water vapor and to the emission current in the ion source. The

partial pressure of water vapor was increased by slowly heating the system. The signal strengths of mass 18 and mass 19 were recorded as the temperature was increased. The emission current of the QMS ionizer was increased from 0.01 to 2.5 mA under constant pressure and, again, the mass 18 and 19 signals were recorded.

If the generation of hydronium is due to ESD the signal at mass 19 should depend on hydrogen coverage at the surface of the ionizer grid. Therefore, the grid was dosed with hydrogen for various amounts of time with the filament on at low emission or completely off. The source of hydrogen was both the background gas at UHV and bottled hydrogen admitted to the system through a leak valve. The filament was then turned back on in the QMS and signals from masses 17, 18 and 19 amu were recorded as time elapsed. This allowed any correlation between these masses and hydrogen dosing to be seen and also allowed the ESD cross-section to be determined.

3.3.3 System description

Mass spectrometer experiments utilized an SRS 200 QMS with channeltron electron multiplier and a custom-built FTMS. They were performed in a stainless steel ultrahigh vacuum system pumped by a 180 L/s (N_2) turbo pump, a 560 L/s (N_2) ion pump and a titanium sublimation pump to a base pressure of 3.8×10^{-10} Torr. A Granville Phillips 307 Bayard-Alpert ionization gauge, calibrated with a MKS spinning rotor gauge, was used to indicate total pressure. The QMS was mounted in close proximity to the FTMS via a 2¾ inch CF tee. The QMS ion source was operated at an emission current of 1 mA, electron energy of 70 eV.

The small and lower resolution FTMS instrument used in the present work was suited for high and ultrahigh vacuum applications. The pulsed electron current was 1uA at lower pressures (< 10^{-8} Torr) and was normally reduced to 100 nA at higher pressures (> 10^{-7} Torr) to avoid space-charge effects. A cylindrical ion trap about 1 cm long and 1 cm in diameter was utilized. An axially parallel magnetic field of approximately 0.45 T from a NdFeB permanent magnet ($\Delta B/B \sim 0.0001$) kept both the electron beam and resulting ions confined to the axis of the cell. This field permits resolution of masses < 0.01 amu apart corresponding to a resolving power of $m/\Delta m >$ 2500. At 19 amu, the minimum resolvable Δm is 0.001 while at 32 amu, the minimum resolvable Δm is 0.003 amu.[3] The ends of the cell were biased at 1.2 V to trap the ions and a 1 to 1.5 V amplitude radio frequency chirp (a few kHz to a few MHz and pulse width of 3 ms) was applied causing all the ions from 1 amu to 190 amu to go into circular motion ($r_{ion} < 0.5$ cm) around the magnetic field lines.[3]

3.4 TOF SIMS

To compliment the previous mass spectrometer experiments, surface analysis was also performed. In order to ascertain the presence and concentration of fluorine and hydronium precursors in stainless steel, a section taken from the stainless steel grid of a QMS ion source was analyzed in a time of flight - secondary ion mass spectrometer (TOF SIMS). The Physical Electronics TRIFT II instrument uses gallium ions (Ga^+) to impact the surface with energy of 15 keV and is capable of resolving 0.001 amu. Both positive and negative ions from the unsputtered and

sputtered surface of an SRS Model 200 QMS grid were examined. The static TOF SIMS analysis was done at a pressure of 3×10^{-10} Torr and the dose was at the static limit (minimal damage to surface during scanning) of 10^{12} ions/cm^2. The reader is referred to Brundle[76] for a more detailed description of TOF SIMS.

3.5 XPS

Using x-ray photoelectron spectroscopy (XPS), the formation of hydronium on the surface of stainless steel can be explored. Several sources[18,65-69] have shown that the signals from oxides and hydroxides can be resolved and that the effects of various processes, such as heating and hydration, change these signals.

3.5.1 Theory

XPS is an important non-destructive surface science tool that analyzes electrons emitted from a material after bombardment with x-rays. It is also known as electron spectroscopy for chemical analysis (ESCA) since it can determine the elemental composition of a surface and to gain information about the chemical state of those elements. The typical depth of analysis is 2 to 5 nm, depending on the material, and can detect down to 0.1% atomic fraction of a particular element. Hydrogen cannot be detected.

X-ray photoelectron spectra are generated by an incident x-ray striking an atom, *A,* and producing an electron, e^-, according to the relation

$$h\nu + A \rightarrow e^{-} + A^{+*} \qquad (3.7)$$

where $h\nu$ is the x-ray photon energy and A^{+*} is the ionized atom in an excited state. The electron is emitted with kinetic energy given by

$$E_{KE} = h\nu - E_b - \phi_{spec} \qquad (3.8)$$

where E_b is the binding energy of the electron in the atom and ϕ_{spec} is the work function of the spectrometer. By calculating the binding energy from the measured kinetic energy, the element that the electron originated from is determined. The actual electron kinetic energy is influenced by several other factors. As the electron leaves the atom, the other electrons in the atom and in surrounding atoms relax, giving a small upward shift in the kinetic energy. Also, the environment of an atom and how it is bound in a solid causes a chemical shift in the energy.

The variance of the binding energy with the chemical environment (valence, electronegativity) of the atom is useful in determining chemical bonding and structure near the surface of materials. In situations where the electron density near an atom is low, the electrons are held more tightly because the nucleus is less screened, giving a shift in the XPS peak toward higher binding energy. A shift toward lower binding energy is observed for atoms with a higher electron density.

In XPS, x-rays are generated by electrons striking a metal anode (usually Al or Mg). In some systems, the x-rays strike a bent crystal monochromator which

focuses the radiation on the sample, eliminates unwanted wavelengths (peaks other than the Mg or Al (Kα) line) and narrows the energy spread. Photoelectrons from the sample pass though a retarding lens where they are focused on the spectrometer entrance slit at a lower energy. The electrons pass through the hemispherical energy analyzer and are focused on a detector that collects the electrons over a range of energies. A schematic of an XPS system is shown in Figure 3.3.

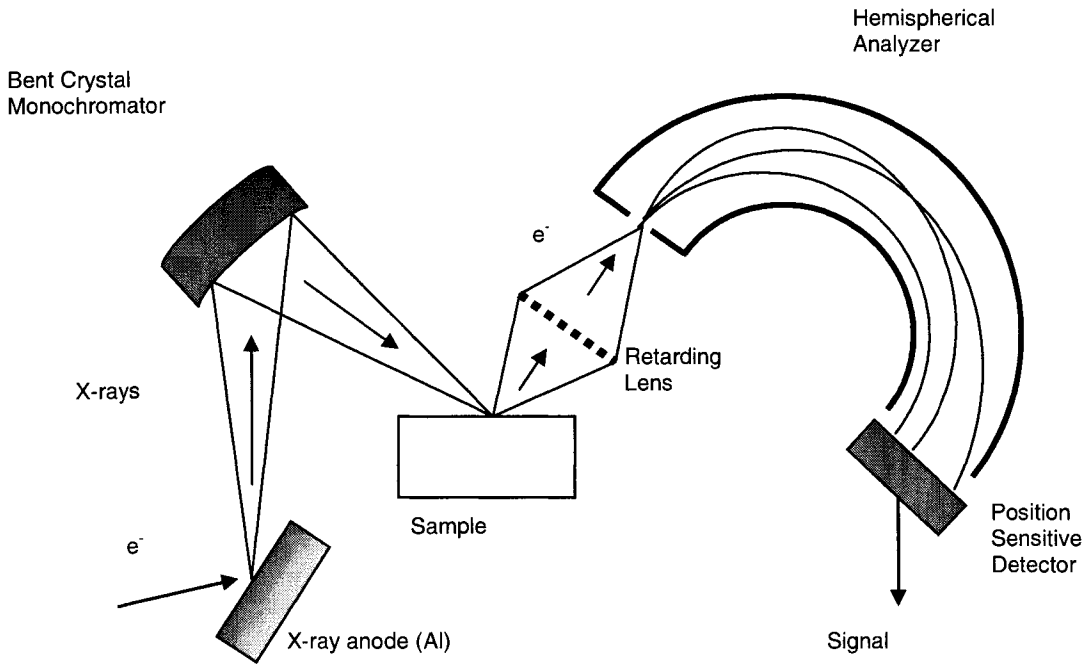

FIGURE 3.3 A simple schematic of an XPS system.

Because the XPS signal is source limited, having more scans improves the signal to noise ratio. Each scan adds to the total number of counts collected and the signal to noise ratio improves as the square root of the number of scans. A typical XPS spectrum of stainless steel is shown in Figure 3.4.

The peaks in XPS spectra are not perfect lines, but are broadened. This broadening is due to the width of the x-ray line itself and detector resolution. The x-rays penetrate the material further than the depth from which electrons can depart and the probability of an electron escaping drops off exponentially with increasing depth. Those electrons that escape after collisions in the material do so with reduced kinetic energy causing a broad background on the higher binding energy side of the peak. Escaping electrons can also interact with other electrons as they leave the sample, yielding secondary peaks.

As electrons escape an insulating material, the surface potential becomes more positive because of the loss of negative charge. This leads to a shift toward higher binding energy over the entire spectrum that is equal to the surface potential. To compensate for surface charging, a low energy flux of electrons can be provided by an electron flood gun to replace those lost by photoemission. In the case of conducting materials, the charge is replaced through the ground connection. Stainless steel has an insulating oxide on its surface; however, it is so thin that charging is not a problem.

By adjusting the angle between the surface normal and the electron escape path, depth analysis can be performed. The intensity will vary as $e^{-z/\lambda\cos\Theta}$, where z is the depth, λ is the mean free path for inelastic electron scattering and Θ is the angle from the sample surface normal. A large value of Θ gives more information about the top surface while a small value includes more information about the subsurface.

In order to quantitatively analyze a material, the relationship between peak intensity and the number of atoms of a particular type must be used, as well as the

photoemission cross section for the particular elements. The peak intensity is given by

$$I = I_x n_i \frac{d\sigma}{d\Omega} P\varepsilon d\Omega \qquad (3.9)$$

where I_x is the x-ray flux, n_i is the number of atoms of a particular type in the sample volume, $d\sigma/d\Omega$ is the differential cross section of the electronic level in that element, P is the probability of escape, ε is the efficiency of the detector and $d\Omega$ is the acceptance angle of the analyzer.

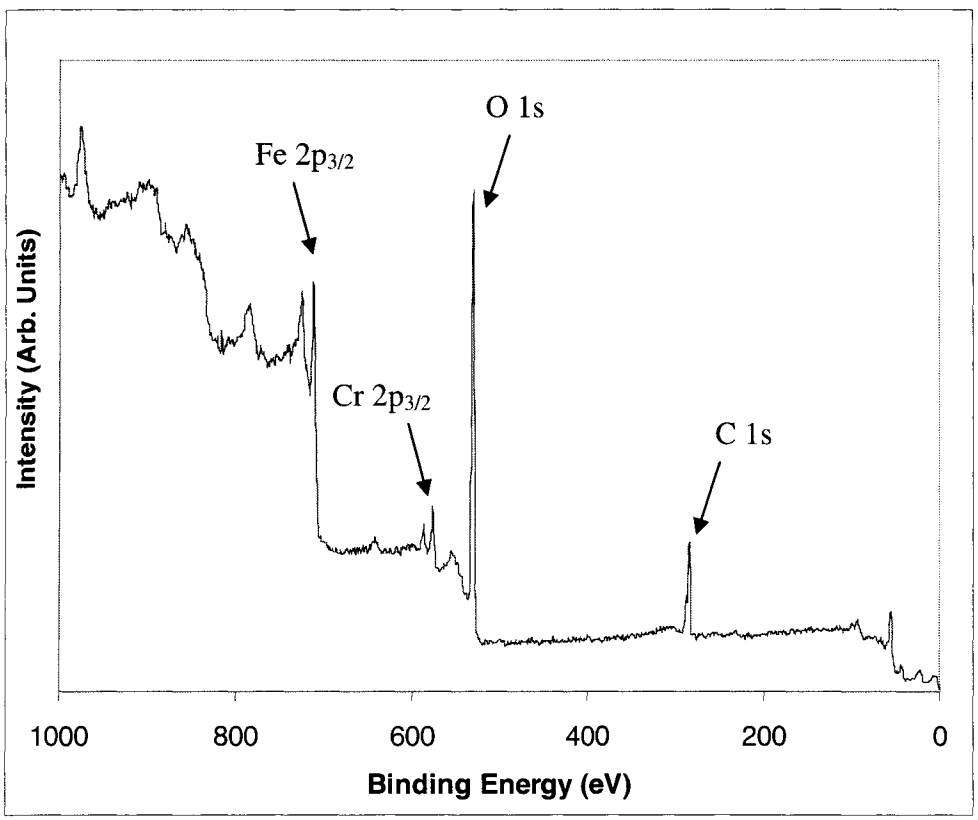

FIGURE 3.4 An XPS survey spectrum of stainless steel.

3.5.2 System description

Data were taken with two separate XPS systems, both having a base pressure $< 1 \times 10^{-9}$ Torr and capability for hydrogen dosing. The XPS system at William and Mary was used to determine the feasibility of examining surface hydroxides and verified the effects of hydrogen dosing. The second system used was the XPS system located at Stanford University, which facilitated sample heating and was equipped with an electron flood gun for electron stimulated desorption experiments. These systems are calibrated using elemental samples (such as gold) and aligning measured peak energies with those known for that element.

The XPS system at W&M was a VG system with an 80 L/s ion pumped analysis chamber. The preparation chamber was pumped using a 100 L/s diffusion pump. A heater assembly with a spring loaded thermocouple was attached to the preparation chamber in order to heat the sample from room temperature to 400 °C. It utilized an Mg anode x-ray source (1253 eV) and electron energies were resolved using a hemispherical energy analyzer, which, at a pass energy of 20 eV, had a resolution of 0.2 eV.

In order to better discern the effects of heating, electron bombardment and hydrogen dosing on the chromium oxide surface, the XPS system located at Stanford was used. A stage was available to heat the sample to over 500 °C in the analysis chamber. Additionally, the system was equipped with an electron gun capable of providing 0.3 mA with the sample biased at 70 eV. For analysis, 1486 eV x-rays from an aluminum anode were used, focused by a bent crystal monochromator onto the

sample at a 35° angle. Photo-electrons had a take-off angle of 35° and their energies were resolved using a hemispherical energy analyzer having a resolution of 0.5 eV at a pass energy of 50 eV.

3.6 XPS Experimental Approach

Coupons of 316L stainless steel (AMS 5507E/ASTM A240/A240M-99A) approx. 10 mm × 10 mm × 0.05 mm and pure (99.99%) polycrystalline chromium approx. 10 mm × 10 mm × 0.5 mm were polished with 3 micron aluminum oxide powder. After a de-ionized water rinse, they were cleaned with acetone in an ultrasonic cleaner. Finally, they were rinsed with a stream of methanol for 1 minute and allowed to dry. Additional samples of unpolished stainless steel were prepared similarly to provide comparative data.

A set of 5 survey scans with a step size of 1 eV were performed followed by 20 scans for Cr $2p_{3/2}$, O 1s peaks and F 1s peaks. Having more scans gives a better signal to noise ratio. In order to cover the entire peak area, the binding energy window used for Cr $2p_{3/2}$ was 565 to 585 eV, for O 1s was 525 to 545 eV and for F 1s was 676 to 696 eV. The step size for the three high-resolution scans was 0.1 eV with a dwell time of 100 ms (the dwell time on the W&M system was 500 ms). For the Cr $2p_{3/2}$ peak, the spot size was 800 × 250 μm and the pass energy was 100 eV, exposing the detector to an energy range of 14 eV. For the O 1s peak, the spot size was 300 μm and the pass energy was 50 eV, giving a detector energy range of 7 eV. For the F 1s peak, the spot size was 1000 × 300 μm and the pass energy was 150 eV, giving a

detector energy range of 20 eV. The larger pass energy and spot size was used in order to get sufficient signal from the small amounts of fluorine present in the samples.

3.6.1 Heating and Hydrogen Dosing

XPS data were taken on the samples of 316L stainless steel and chromium as received, after heating the samples to over 400 °C for three hours and after different amounts of hydrogen dosing. The dosing was accomplished by cumulative exposure: first exposure to the background vacuum overnight, then by backfilling with hydrogen to 1×10^{-7} Torr for three hours, exposure to the background vacuum overnight again and then after backfilling for three more hours.

A second 316L stainless steel sample was heated, increasing the temperature by 100 °C every half hour, from room temperature up to 500 °C. XPS surveys and scans of the Cr $2p_{3/2}$ and O 1s peaks were taken after each step. Additionally, the F 1s peak was scanned at room temperature and 500 °C. The sample was allowed to cool in vacuum and then exposed to atmosphere for 8 hours. XPS data were taken after each of these time periods.

3.6.2 Electron bombardment

Experiments were also conducted to determine the effects of electron bombardment of stainless steel and chromium. XPS data were taken on stainless steel

before electron bombardment, after 5 hours of bombardment, and also after 8 hours of bombardment with 0.3 mA of 70 eV electrons. The same was done for chromium except that electron bombardment was only done for 5 hours due to time constraints.

CHAPTER IV

FTMS RESULTS AND DISCUSSION*

Ion cyclotron resonance (ICR) Fourier transform mass spectrometry (FTMS) was selected as one method to determine the identity of the mass 19 peak because of its very high resolution. Also, the gas phase formation of hydronium can be studied using an FTMS spectrometer, since ionization times and reaction times can be adjusted by modifying control software. FTMS was used to resolve the contributors to the signal at mass 19 amu, in order to show that hydronium is a possible source. The resolution of the instrument was demonstrated, fluorine and hydronium were resolved and the effects of water concentration on hydronium formation were explored.

In order to verify the resolution of the FTMS system, spectra of selected gases with similar mass were obtained using the sequence described in section 3.3.1. First, in Figure 4.1, the signal seen at mass 15 is not only due to CH_3^+ to which it is usually attributed, but it is also due to NH^+ from the residual gas background. Figures 4.2(a)-(c) show resolution of CO^+ and N_2^+ ($\Delta m = 0.011$ amu), O_2^+ and S^+ ($\Delta m = 0.018$ amu) and H_3O^+ and F^+ ($\Delta m = 0.020$ amu). The peaks were all verified by increasing the partial pressure of the source gases from a system ultimate pressure of 2×10^{-8} Torr. The H_3O^+, N_2^+ and O_2^+ were generated from admission of air, the CO^+ was generated

* Significant portions of this chapter taken from Cole et al., JVST A 21 (5), Sep/Oct 2003

as a fragment of CO_2 and S^+ was obtained from SF_6 and F^+ from CF_4. As shown in Figure 4.2(d), a preliminary frequency chirp (see section 3.1.1) that ejects all ions except those at or near mass 19 minimizes space charge effects, increases dynamic range and greatly improves the signal to noise ratio (compare Figures 4.2c and 4.2d).[3]

In order to ascertain the makeup of mass 19, admission of a fluorine bearing gas was required, since no fluorine was detectable in the residual gas of the vacuum system. Admission of SF_6 into the system to a pressure of 5.6×10^{-6} Torr showed no increase at 19 amu. Consistent with past fragmentation patterns,[77] however, admission of CF_4 did give a small F^+ signal, but only 0.4% the height of the major CF_3 peak. To create a greater number of fluorine ions, the partial pressure of CF_4 was increased to 2.1×10^{-6} Torr and the electron current was increased to 120 nA. Figures 4.3(a)-(c) show an increase in the height of the F^+ peak relative to the H_3O^+ peak as the partial pressure of CF_4 is increased.[3]

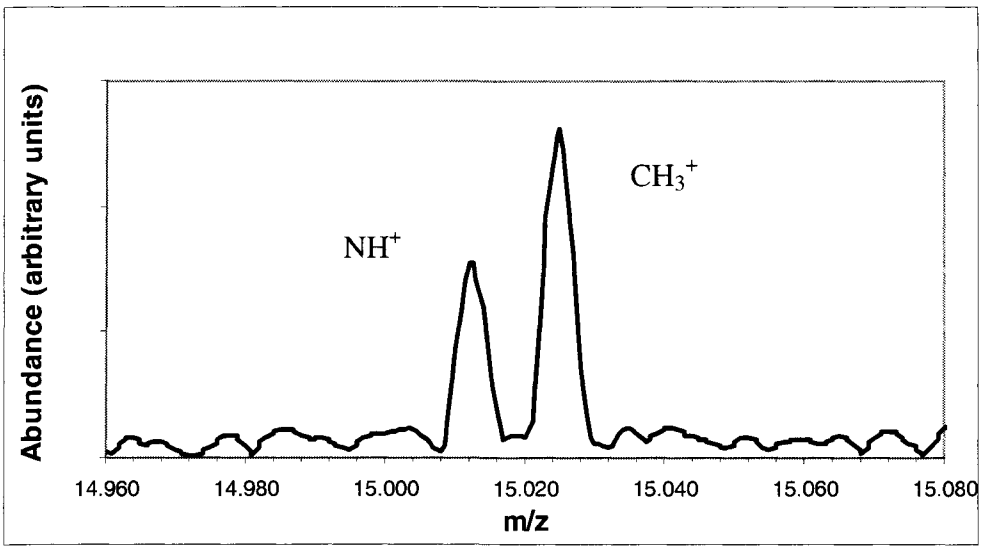

FIGURE 4.1 A high resolution FTMS spectrum near 15 amu shows contributions from NH^+ as well as CH_3^+.[3]

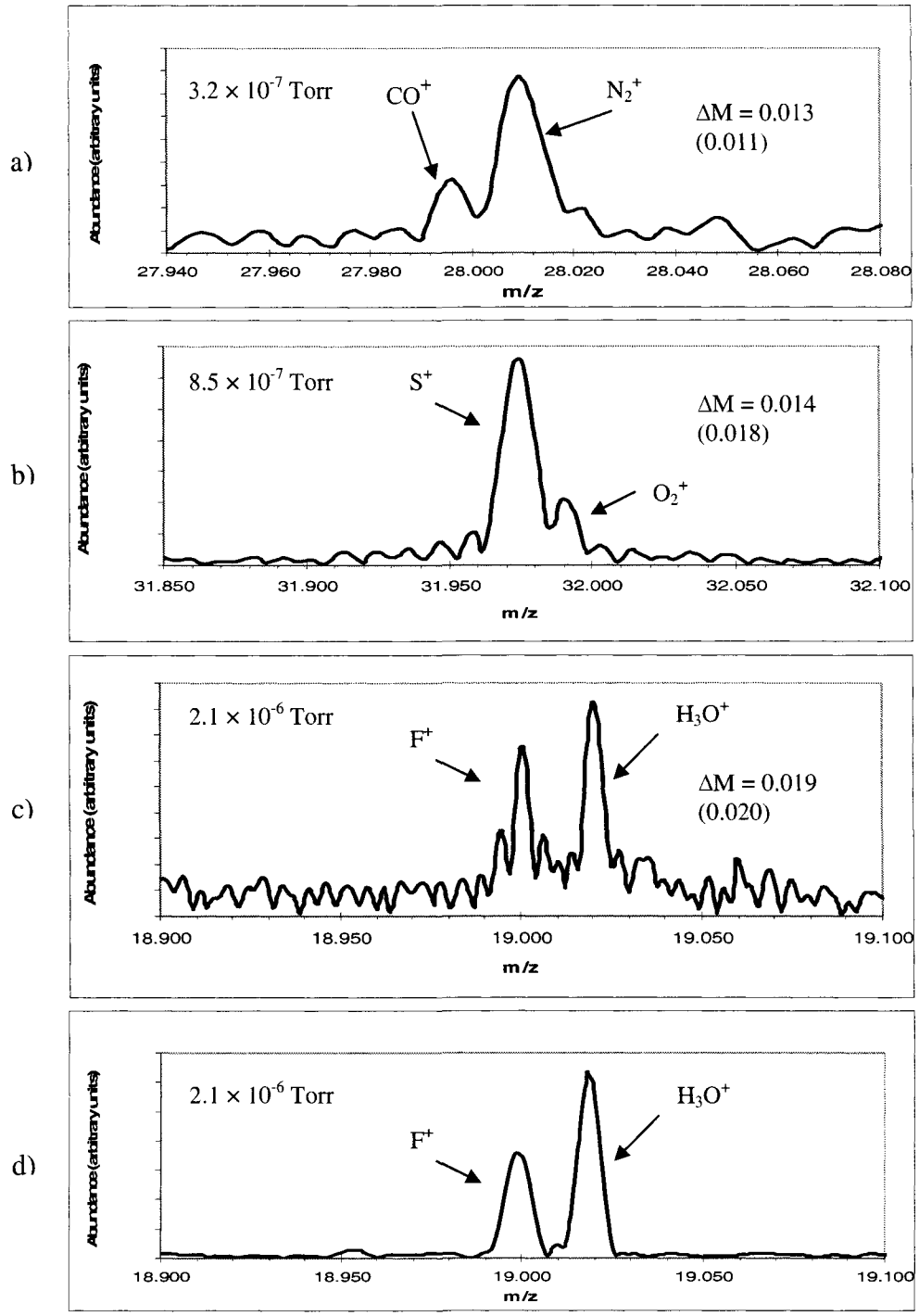

FIGURE 4.2 Using FTMS, high resolution mass spectra showing the separation between (a) N_2^+/CO^+, (b) O_2^+/S^+ and (c) F^+/H_3O^+ is possible. The numbers in parentheses are the theoretical mass differences between the most abundant isotopes. Figure 4.2(d) shows the resolution of F^+/H_3O^+ with better signal to noise ratio obtained by ejecting all ions except those at or near 19 amu.[3]

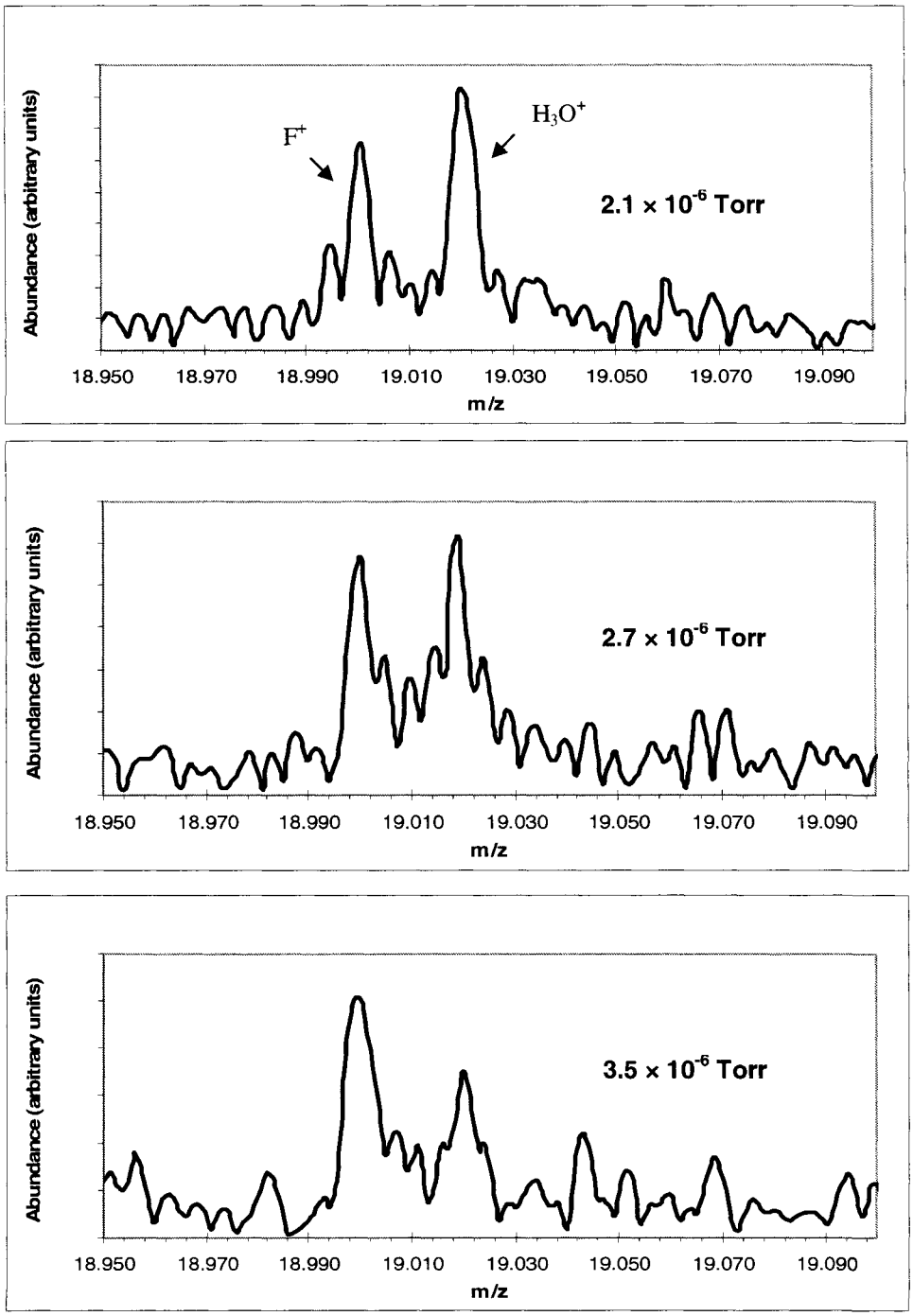

FIGURE 4.3 High resolution mass spectra of F^+ and H_3O^+ were obtained as the partial pressure of CF_4 was increased. At total pressures of (a) 2.1×10^{-6}, (b) 2.7×10^{-6} and (c) 3.5×10^{-6} Torr, respectively, the spectra show that the ratio of fluorine to hydronium increases in relation to the partial pressure of CF_4.[3]

To further characterize mass 19, parametric studies of signal versus water partial pressure were conducted. The system was baked to 120 °C for 12h to reduce the pressure, but allow enough gas phase water to remain for comparison experiments. By heating the vacuum envelope slightly and gradually, the partial pressure of water was increased. As seen in Figure 4.4, at pressures near 1×10^{-7} Torr, the ratio $[H_3O^+]/[H_2O^+]$ linearly increases as a function of the H_2O partial pressure from zero up to ~0.25 at 8×10^{-7} Torr. This is what one would anticipate if H_3O^+ is produced from gas phase reaction involving water vapor. The amount of OH^+ stays constant initially, but begins to decrease as the partial pressure of water increases beyond 5×10^{-7} Torr (shown later in Figure 5.4b). This decrease is most likely due to space charge suppression of the signal since the hydronium signal starts to become non-linear as well.[3]

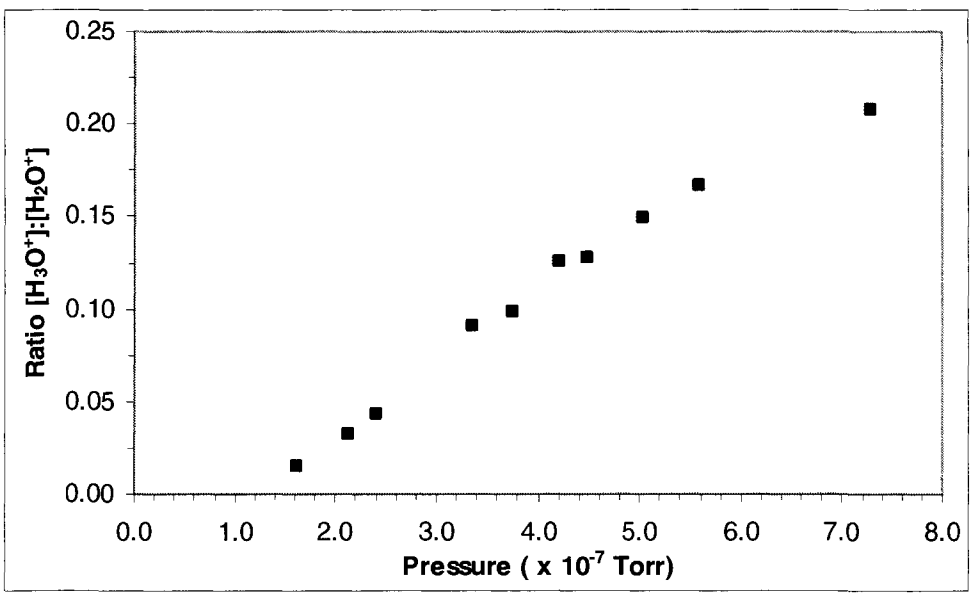

FIGURE 4.4 The ratio of H_3O^+ to H_2O^+ as observed in the FTMS spectrum is presented as a function of the partial pressure of H_2O in the vacuum system.[3]

Generation of hydronium can occur through the exothermic reaction of Equation (1.1) as stated again here

$$H_2O^+ + H_2O \rightarrow H_3O^+ + OH \qquad (1.1)$$

This reaction has been rather well studied.[78-82] The experimental observations can be summarized as follows: (a) The thermal rate constant, k, for this reaction has been measured by several groups and found to be in the range k =1.7 - 2.5 $\times 10^{-9}$ cm^3/sec.[78-80] (b) Rate constant measurements at collision energies of a few eV show that *k* remains constant or increases slightly from its thermal value.[80,81] (c) Detailed studies of the kinematics of Equation (1.1), for collision energies of a few eV, reveal that the reaction proceeds via H atom transfer, proton transfer, and intermediate complex formation in roughly equal proportions.[82]

It is helpful to consider an example relevant to the operating conditions of the present FTMS cell: at a H_2O partial pressure of 2.4 $\times 10^{-7}$ Torr, the ratio R = $[H_3O^+]/[H_2O^+]$ was found to be 0.044. The generation of H_3O^+ is governed by

$$\frac{d[H_3O^+]}{dt} = k[H_2O^+][H_2O] \qquad (4.1)$$

and the ionization rate,

$$[H_2O^+] = \alpha\,[H_2O]\,t \qquad (4.2)$$

For small values of R,

$$R = \frac{[H_3O^+]}{[H_2O^+]} \approx \frac{k}{2}[H_2O]\tau \qquad (4.3)$$

where τ is the time available for transforming the H_2O^+ formed in the initial electron ionization pulse into detectable H_3O^+. If we take $k = 2 \times 10^{-9}$ cm^3/s, T = 300 K and $[H_2O] = 8.4 \times 10^9$/cm^3, then Equation (4.3) gives $R = 8.4\ \tau$, implying that a time of at least $\tau = 5.2$ ms is required to produce the observed value of R. In the current apparatus, the ionizing electron beam is "on" for 20 ms, allowing ample time for the required conversion of H_2O^+ into H_3O^+ in the gas phase. Subsequent conversion of H_2O^+ to H_3O^+ may also occur during the trap and resonance periods (described in sections 3.1.1 and 3.3.1) after the electron beam ionizing pulse is terminated.[11]

From Equation (4.3), it is obvious that the ratio, R, should increase with the partial pressure of H_2O. As was shown in Figure 4.4 there is an approximately linear behavior of R as a function of the partial pressure of H_2O. It is clear that these results are compatible with the predictions of Equation (4.3). The offset that is seen in Figure 4.4 is attributed to the inherent capacitance of the system electronics, which results in a minimum detectable number of ions and the relatively small signal-to-noise ratio. Pathways leading to the destruction of the H_3O^+ ions are not considered in this analysis and may be responsible for the slight negative curvature of R vs. pressure exhibited in Figure 4.4.[11]

It is important to contrast the present FTMS observations with what would be observed in a quadrupole mass spectrometry (QMS) instrument. The rate equation

(4.3) indicates that the hydronium concentration is proportional to both the number density of H_2O^+ and the time available for formation. Although the time in the FTMS to permit gas phase generation of H_3O^+ is long (ionization, trap and resonance ~ 30ms), the ionization current is typically on the order of 100 nA pulsed. The emission current of most QMS instruments is ~1 mA continuous, a factor of ~10^4 greater, but the ion extraction time and, therefore, the time for H_3O^+ formation, is only a few μsec. Using these values at VHV (~ 1×10^{-7} Torr), H_3O^+ production is a factor of 7×10^3 greater in the FTMS compared to the ion source of a QMS instrument, suggesting that production of H_3O^+ in a QMS could not account for the signal at 19 amu. However, the overall sensitivity of a QMS with an electron multiplier is substantially higher (> 1000 times) so that detection of an H_3O^+ peak produced via the gas-phase ion-molecule reaction given in Equation (1.1) appears possible.

Clearly, signals from fluorine and hydronium can be resolved using an FTMS instrument. Hydronium production is predominately a gas-phase process in this type of instrument, but its formation in a QMS instrument is also possible. Since a peak is often detected at mass 19 in a QMS, the behavior of this "anomalous" peak is explored in the next chapter.

CHAPTER V

QMS RESULTS AND DISCUSSION*

In the preceding chapter, the presence of hydronium in a Fourier transform mass spectrometer (FTMS) was verified and H_3O^+ detection in a quadrupole mass spectrometer (QMS) was deemed plausible. Using a QMS, the characteristics of the mass 19 peak were explored and the effects of hydrogen dosing were noted.

The spectra of the QMS and FTMS mass spectrometers from 0 - 50 amu are compared in Figure 5.1. The setup was described in section 3.3.3. The QMS spectrum taken at a pressure of 4×10^{-10} Torr is shown in Figure 5.1(a) where the intensity of the mass 19 peak was seen to be significant, about 30% of that for mass 18. Figure 5.1(b) shows a corresponding FTMS spectrum which indicates that the signal observed at mass 19 is H_3O (19.02 amu). No fluorine or other peaks near m/e ~ 19 were noticeable.

As shown in Figure 5.2, when the water vapor concentration in the vacuum system was increased (accomplished by heating), the QMS showed a roughly linear increase in mass 18. Simultaneously, the mass 19 signal stayed relatively constant up to about 9×10^{-10} Torr in pressure, implying that it was not primarily generated by a gas phase mechanism involving water at these pressures.

---

* Significant portions of this chapter taken from Cole et al., JVST A 22 (**5**), Sep/Oct 2004

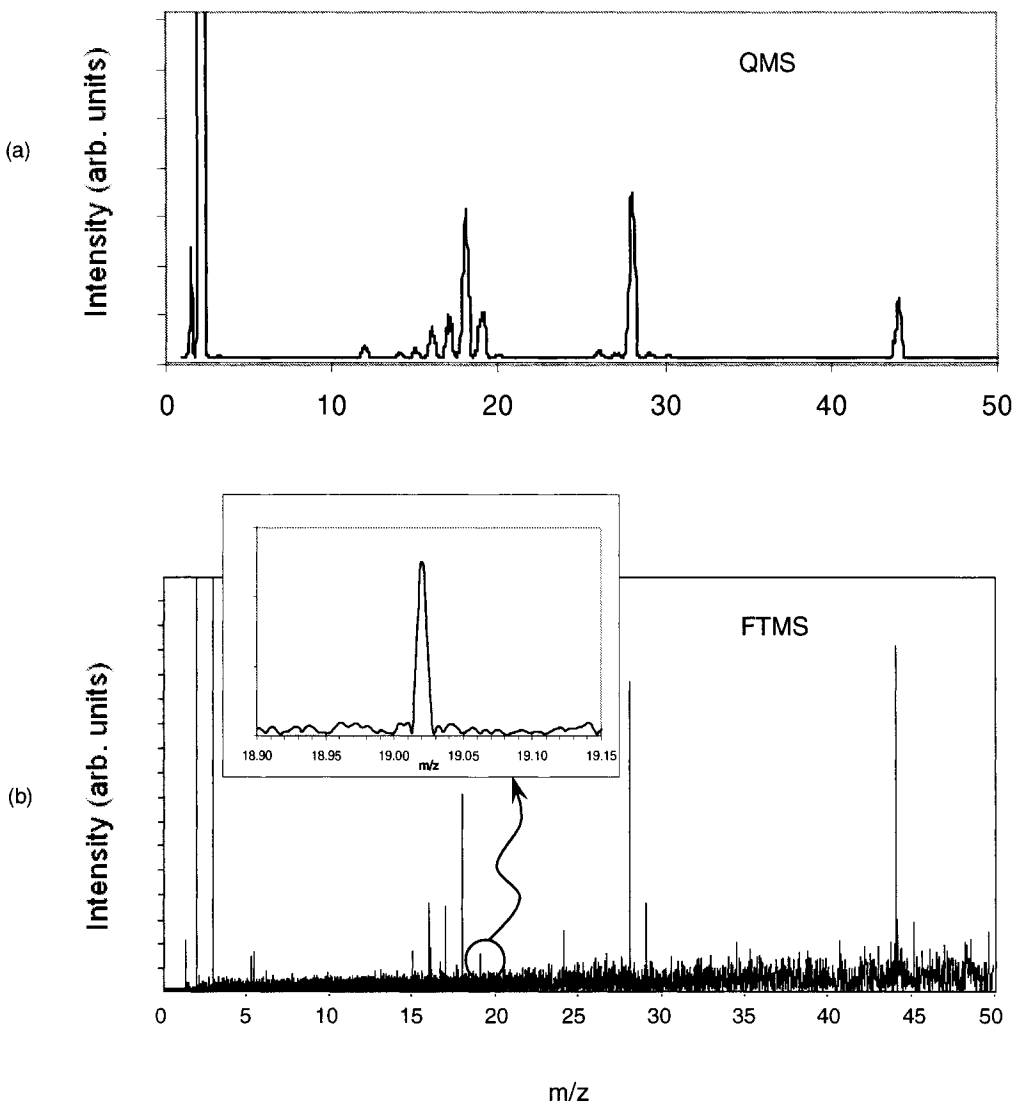

FIGURE 5.1 A standard QMS mass spectrum at ~4 × 10^{-10} Torr over 0 – 50 amu (a) is illustrated along with that for a high resolution FTMS mass spectrum at ~1 × 10^{-8} Torr (b). The inset in (b) shows that the signal is H_3O^+, with a mass of 19.02 amu.[11]

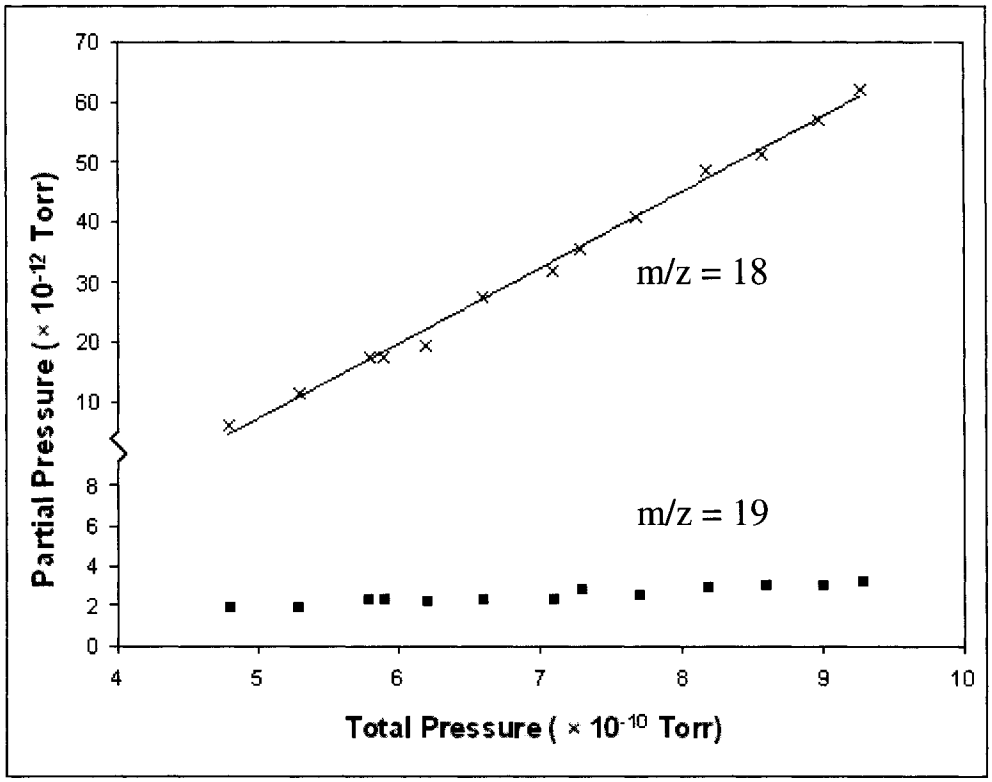

FIGURE 5.2 The signal in the QMS at mass 19 is shown to remain relatively constant as the partial pressure of water is increased in the system. This indicates that the signal is not generated in the gas phase, but, rather, is a result of ESD.[11]

The notion that mass 19 is formed via electron stimulated desorption (ESD) was tested by varying the emission current in the QMS ionizer from 0.01 mA to 2.5 mA at a constant pressure of 4×10^{-10} Torr. Figure 5.3 shows that the height of the mass 19 peak varied linearly, as would be expected from the equation

$$J_o = \sigma \Theta N_o J_e \qquad (5.1)$$

where J_o is the ESD ion flux, σ is the ESD cross-section, Θ is the surface coverage, N_o is the monolayer concentration and J_e is the incident electron flux density. Because

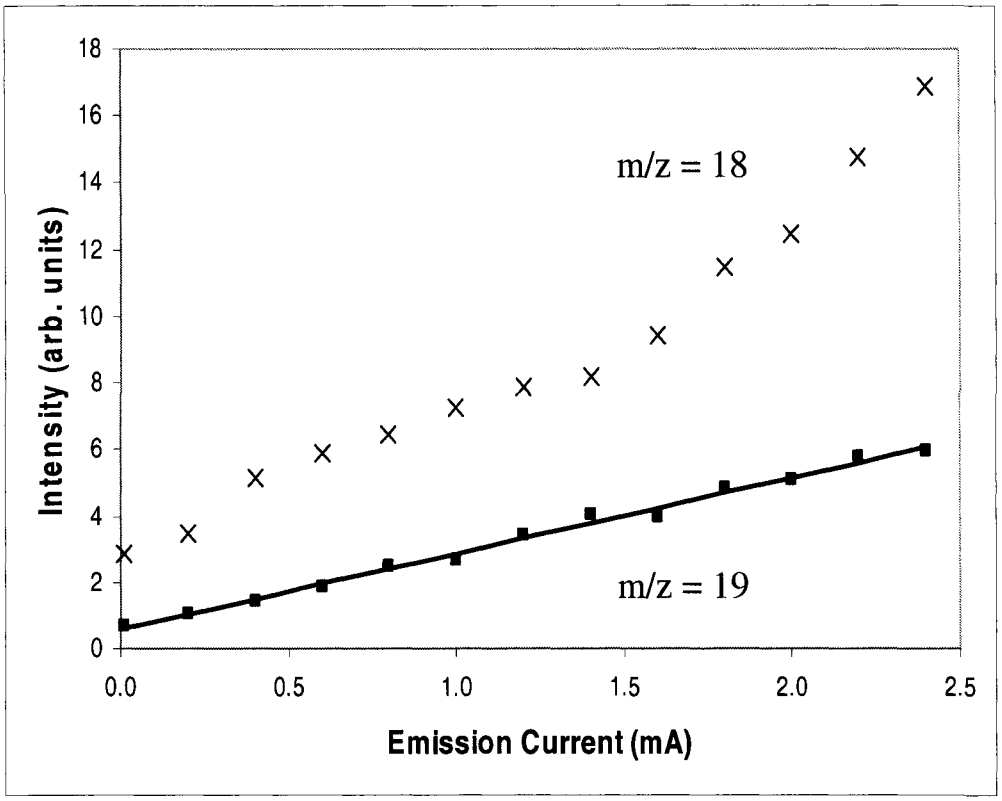

FIGURE 5.3 The linear behavior of the mass 19 signal with emission current supports the premise that mass 19 arises from ESD of the grid.[11]

the previous experiment (Figure 5.2) showed that mass 19 was not being generated in gas phase interactions, since it did not significantly increase with H_2O pressure increase, it appears that H_3O^+ is most likely generated by ESD. More evidence of this assertion is shown in Figure 5.4(a). As expected, the ratio of mass 17 (OH^+) to mass 18 (H_2O^+) stayed relatively constant as the partial pressure of water vapor in the vacuum system was increased. The ratio of mass 19/18, however, decreased. The most consistent explanation is that the amount of water in the gas phase increased and the ESD generated signal at mass 19 stayed relatively constant. As the pressure increased above 9×10^{-10} Torr, the ratio tapered off to a steady state value. This steady state value may incorporate the related rates of re-adsorption of H_2O onto the

grid and desorption of H_3O^+ by ESD. At even higher pressures, the contribution to the mass 19 signal from gas-phase hydronium may increase. Figure 5.4(b) shows the mass 19/18 ratio, $[H_3O^+]/[H_2O^+]$, at the higher pressure for the FTMS. The ratio increased linearly as a function of the H_2O partial pressure from zero up to about 0.25 at 8×10^{-7} Torr. This is anticipated if H_3O^+ is produced from a gas phase reaction involving water vapor. This increase in hydronium production could also occur in the QMS as discussed in Chapter IV.

Assuming that hydronium generation in UHV occurs predominately via ESD, the signal at mass 19 should increase as hydrogen accumulates on the surface of the ionizer grid. After the ionizer grid was degassed, the system was dosed with hydrogen at 1.0×10^{-8} Torr for 2 minutes for a cumulative exposure of approximately 1 Langmuir. The exposure was performed with the filament both off and on at 0.01 mA emission. There was no discernable change in the mass 19 signal level in either case, which may indicate that more time is required to form the precursors of hydronium (possibly adsorbed H_2O or metal hydroxides). Additional exposure of the grid to H_2 (with the ionizer filament turned off) was achieved by allowing it to accrete from the predominantly hydrogen background vacuum of 4×10^{-10} Torr for 12 hours (~17 Langmuir). The filament was then turned back on at 1 mA emission and the signals for mass 17, 18 and 19 all started out at a higher value than the baseline, as may be seen in Figure 5.5. The signals of mass 17 and 18 increased for several minutes as thermal desorption of water from the grid and surrounding walls occurred, undoubtedly due to the increase in temperature associated with the radiant energy of the filament.

(a)

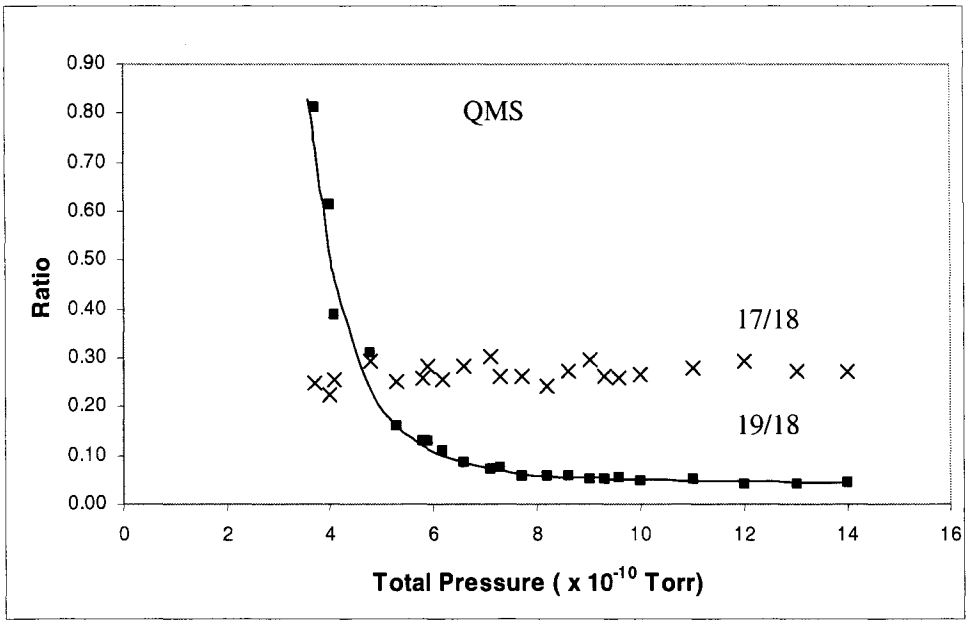

(b)

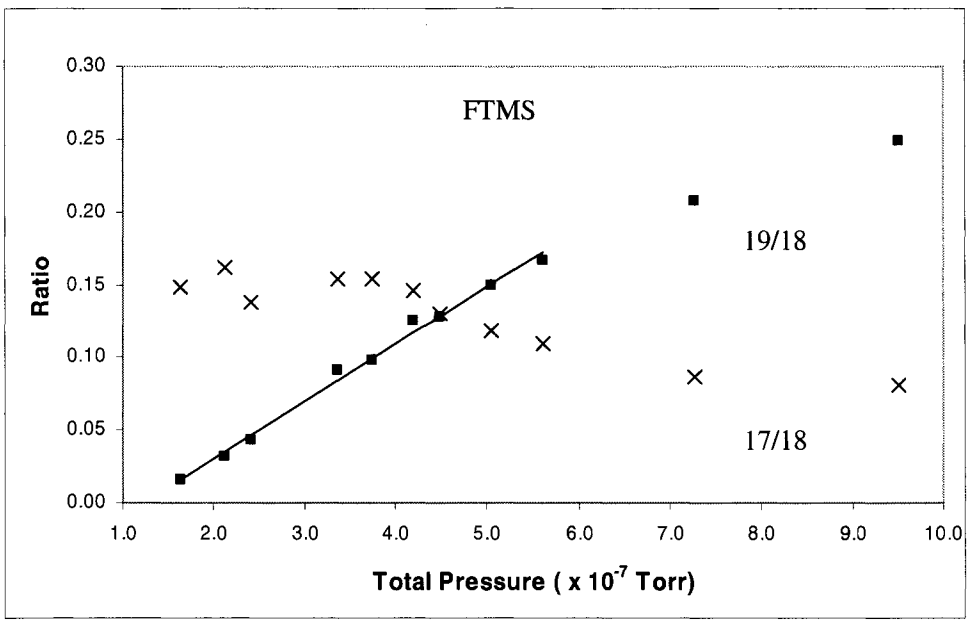

FIGURE 5.4 (a) In a QMS, when the partial pressure of water is increased sufficiently, the ratio of mass 19 to mass 18 (squares) decreases and eventually reaches a steady state value, while the ratio of mass 17 to mass 18 remains constant. There is a crossover pressure (~10^{-9} Torr) where mass 19 begins to track mass 18. (b) The lower plot shows the behavior of these same ratios in an FTMS instrument at much higher pressure where the ratio 19:18 actually increases with increasing pressure owing to the dominant source of H_3O^+ arising from equation (1.1). The lines shown are not a best fit, but are there to aid the eye.[11]

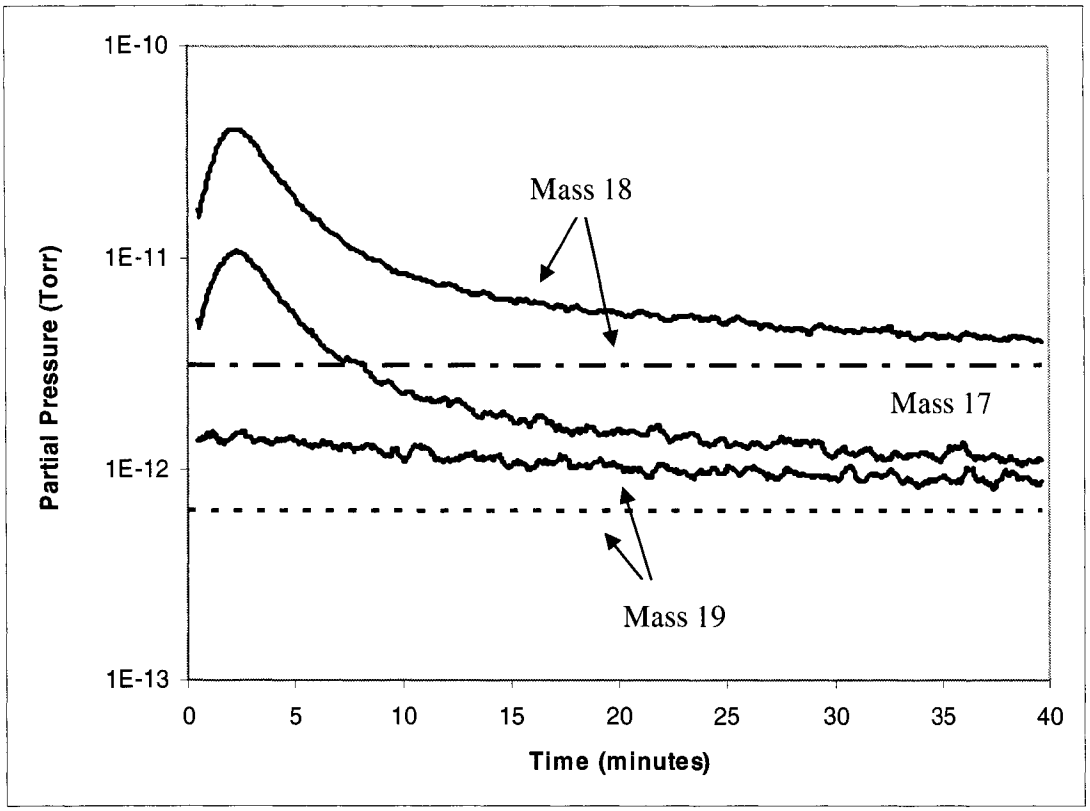

FIGURE 5.5 The filament is turned off for 12 hours at a pressure of ~ 4×10^{-10} Torr (H_2) and then turned on at 1 mA emission. The signals for mass 17, 18 and 19 all start higher than before the filament was extinguished (dashed lines). Mass 17 and 18 initially increase (grid desorption) while mass 19 decreases.[11]

Simultaneously, however, the mass 19 signal started to decrease. This behavior indicates ESD generation instead of the gas-phase generation of mass 18. After increasing the emission current to 2 mA for one hour and then returning it to 1 mA, the mass 19 signal was lower, probably because the surface source of hydronium was reduced with a higher rate of ESD. The emission current was then reduced to 0.01mA for one hour. When the emission current was subsequently increased from 0.01 mA to 1 mA, the mass 19 signal increased by over 20% and then slowly decayed

to a steady state value, most likely because its source had increased during the time of reduced emission and lower ESD rate.

In an additional test to confirm the origin of mass 19 in the QMS, the grid was saturated with hydrogen for 8 hours at 1×10^{-6} Torr and then pumped back down to the base pressure of about 4×10^{-10} Torr . Figure 5.6 shows that the mass 19 signal is nearly 6×10^{-12} Torr initially and then begins to decrease by a factor of 10 as the hydrogen is depleted. The lower portion of the curve probably represents rate limited H diffusion from the bulk, which supplies the surface ESD process.

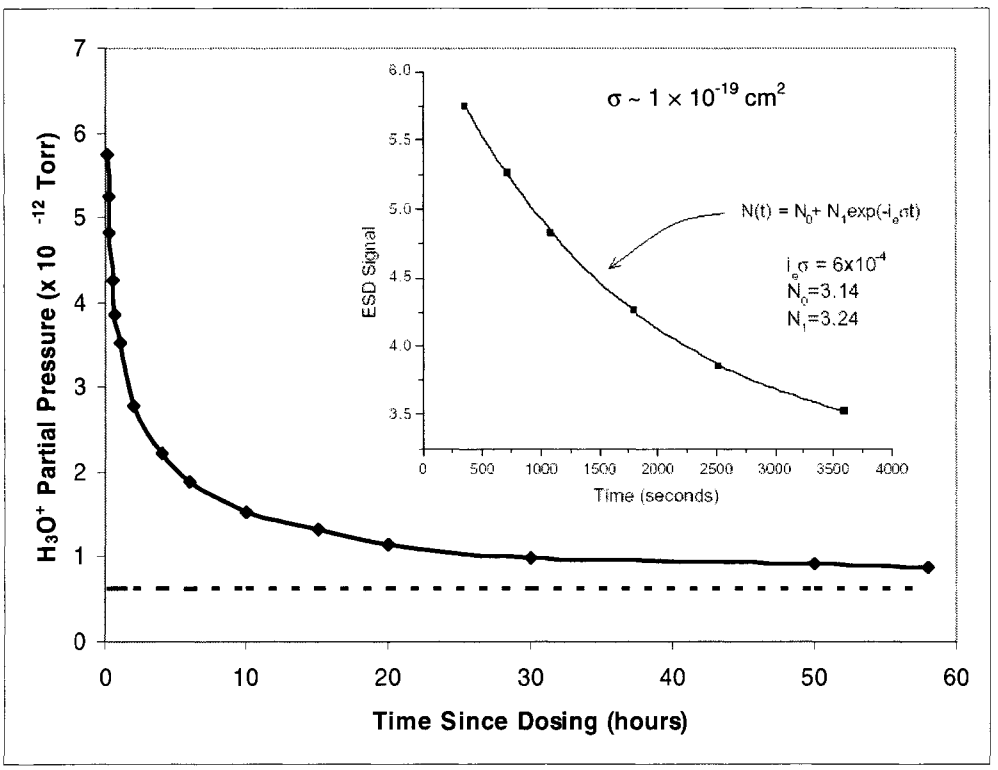

FIGURE 5.6 After hydrogen is allowed to saturate the system components for 8 hours at 1.0×10^{-6} Torr, the signal at mass 19 increases by 10× from its pre-dose value (dashed line). The signal then begins to decrease over time. Inset is the first six points from which the ESD cross section $\sigma \sim 1 \times 10^{-19}$ cm^2 is estimated.[11]

Even though the actual mechanism has not yet been determined, it is instructive to estimate the overall cross section for the ESD hydronium reaction. With an estimated ~ 1 cm^2 grid area impacted by electrons, the ESD cross section for the initial rate was determined to be ~1×10^{-19} cm^2. This is shown in the inset of Figure 5.6. If approximate monolayer coverage of a surface hydroxide complex, 1×10^{15} atoms/cm^2, is assumed, the formation efficiency is 1×10^{-4} ions/e.

TABLE 5.1 Time of Flight SIMS data from a stainless steel grid of a mass spectrometer ion source. Numbers are in counts per million of total sputtered constituents. Principle species of the stainless steel are Fe, Cr, and Ni.

	Positive Ions		**Negative Ions**	
Atom/Molecule	**As received**	**Sputtered**	**As received**	**Sputtered**
H	**41686 (4.2%)**	**16702 (1.7%)**	**419310 (42%)**	**137499 (14%)**
O	**34 (.0034%)**	**76 (.0076%)**	**189867 (19%)**	**278279 (28%)**
OH	**23 (.0023%)**	**52 (.0052%)**	**68804 (6.9%)**	**109446 (11%)**
H_2O	**11 (.0011%)**	**13 (.0013%)**	**310 (.03%)**	**458 (.05%)**
H_3O	**53 (.0053%)**	**27 (.0027%)**	**---**	**---**
F	**---**	**---**	**880 (.09%)**	**2507 (.25%)**
Na	**24396 (2.4%)**	**221445 (22%)**	**---**	**---**
K	**8030 (.8%)**	**101472 (10%)**	**---**	**---**
^{35}Cl	**---**	**---**	**3627 (.36%)**	**41415 (4.14%)**
^{37}Cl	**---**	**---**	**1183 (1.18%)**	**13398 (1.33%)**

Table 5.1 shows the results of the TOF SIMS experiment performed on the stainless steel grid of the mass spectrometer. The concentrations of the positive ions Na^+ and K^+ (possible constituents of metal halides) were observed to be 2.4% and 0.8% respectively. After sputtering away the surface layers, the magnitudes increased by about an order of magnitude. H^+ was detected at about 4%, but decreased by more than a factor of 2 after 35 seconds of sputtering (several monolayers). This suggests that the concentration of H in the surface complex was greater than in the bulk of the

stainless steel. Also, trace amounts of O^+, OH^+, H_2O^+ and H_3O^+ were detected (< 0.01%) as expected, but no F^+ was detected. Figure 5.7 shows unambiguously the presence of a small number of positive hydronium ions at 19.020 amu, but no positive fluorine ions (18.998 amu) are present (F^+ normally presented as the source of mass 19 in a QMS).

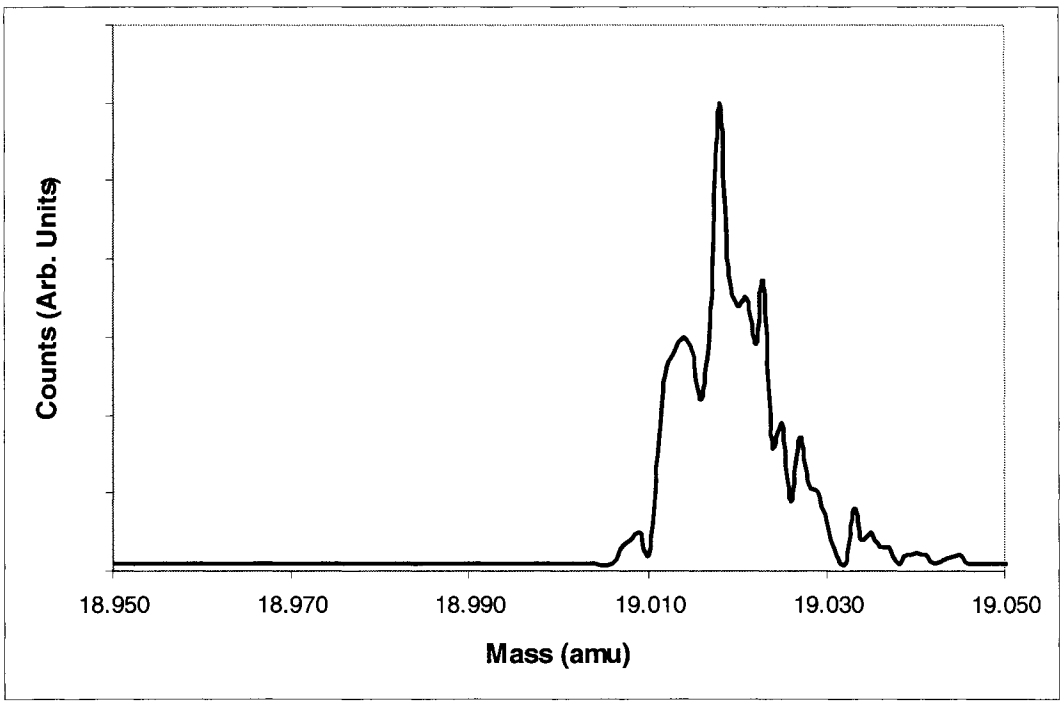

FIGURE 5.7 TOF SIMS positive ion spectrum near 19 amu shows the presence of hydronium (mass 19.020 amu), but no indication of fluorine (mass 18.998 amu).

In the negative ion mode, Cl^- and F^- were observed. After sputtering, Cl^- increased from 0.5% to over 5% and F^- increased from 0.1% to 0.25%, but these amounts were much less than that observed for H^-, O^-, OH^- and Na^+. The amount of H^- detected was reduced from over 40% to less than 14% after sputtering while O^- and

OH^- increased from ~19% to 28% and ~7% to 11%, respectively. These numbers indicate that the precursors to hydronium (H, O and OH) are much more prevalent than F at the surface of stainless steel. Also, the disproportionate amount of Na and K makes metal halides an unlikely source of F^+ and mass 19 signals in a QMS.

Most investigations assume ESD generated mass 19 ions to be F^+, since it is the simplest specie with that mass. They have offered differing opinions for the ESD mechanism which produces mass 19 amu[22-25] and its kinetic energy distribution.[9,35,39,45,83] As described in section 2.2, the Menzel-Gomer-Redhead (MGR) model describes desorption due to excitation to an ionic anti-bonding state whereas the Knotek-Feibelman (KF) model describes desorption via Auger decay. Either model might be applicable, depending on the surface. As for the source of F^+, some investigators suggest the migration of fluoride molecules within a system[14] or fluorine transfer between surfaces[34], and even mention allowing the substrates involved to "accrete fluorine from the system background,"[35] all of which would probably yield a gas-phase signal as well.

The evidence from the work presented in Chapter IV and in this chapter indicates that the mass 19 signal is H_3O^+, not F^+. The TOF SIMS results clearly show the presence of H^+, OH^+, H_2O^+ and H_3O^+, but no F^+ in the positive ion spectra sputtered from the grid. Even in the negative ion spectra, the components of hydronium are far more prevalent than F^-. From the QMS results, the mass 19/18 ratio, shown in Figure 5.4(a), decreases as the pressure increases to ~ 9×10^{-10} Torr (H_2O), after which the ratio remains constant at 0.04, clearly indicating that the source of mass 19 is not water in the gas phase. Figure 5.5 shows mass 19 does not

follow water desorption from the grid, but, instead, decays monotonically from the depletion of some surface complex, possibly a metal hydroxide. Further, when the grid was saturated with hydrogen, the ESD hydronium signal increased tenfold (see Figure 5.6). The cross section $\sigma \sim 1 \times 10^{-19}$ cm^2 shown in the inset of Figure 5.6 is near the lower part of the range of first order ESD cross sections that have been observed previously (typically 10^{-16} to 10^{-20}), such as H^+ from stainless steel (1.3×10^{-16} cm^2),[12] "fluorine" (possibly hydronium) from stainless steel (9.6×10^{-18} cm^2) [12] and H_2O^+ from Mo (~ 10^{-17} cm^2).[84]

Hydronium formation via a surface process has been proposed before[10] and, in fact, observed in earlier field desorption experiments.[85] Hydronium generation in an electron impact source has been documented[86] and its formation through the reaction

$$H_2O^+ + H_2 \rightarrow H_3O^+ + H \qquad (5.2)$$

has been suggested, where the source of the hydronium is not solely water and water ions, as in the more recognized gas phase reaction as stated earlier

$$H_2O^+ + H_2O \rightarrow H_3O^+ + OH. \qquad (1.1)$$

The existence of water clusters and higher order hydrated proton clusters ($H_7O_3^+$, $H_9O_4^+$, etc.) on surfaces is well accepted.[72] With the constant motion of molecules on the surface and the propensity to form hydrogen bonds, the structure of

water as individual H_2O molecules may be the least probable configuration. Hydronium ions could very well be formed on a surface by a first order electron ionization, but a second order process cannot be ruled out. Experiments by Beavis[62] and Funke *et al*,[63] have shown that water can form when surface oxides of stainless steel are exposed to hydrogen. Formation of metal hydroxides is also a possibility. The surface of heated stainless steel in vacuum is predominantly, Cr_2O_3 and with hydrogen saturation may form $Cr(OH)_3$ from which H_3O^+ may be generated.

It has been shown that the source of mass 19 in a QMS at ultra high vacuum is primarily a surface ESD process. There is also ample evidence that chemical activity involving hydrogen, oxygen and water occurs on the surface of stainless steel. Therefore, it is interesting to consider the chemical changes that occur on this surface when heated, hydrogenated and bombarded with electrons using the technique of x-ray photoelectron spectroscopy.

CHAPTER VI

XPS RESULTS AND DISCUSSION*

In the previous chapter, it was shown that hydrogen dosing the stainless steel grid of a quadrupole mass spectrometer (QMS) increased the electron stimulated desorption (ESD) generated mass 19 signal. This is consistent with the surface of stainless steel being chemically active[62,63] in spite of the formation of a stable oxide at its surface, as discussed in section 2.3. In this chapter, x-ray photoelectron spectroscopy (XPS) is used to study the effects of heating and electron bombardment on the composition and surface chemistry of stainless steel and chromium oxide. We will see that these processes tend to reduce the amount of hydroxide complexes found on the surface, supporting the premise that ESD hydronium contributes to the mass 19 signal in mass spectrometers.

6.1 General Results

Using XPS analysis as described in sections 3.5 and 3.6, the composition of the surface of polished stainless steel was explored. Fluorine and hydroxides were of particular interest, including how they interacted with other species. The XPS survey scan showed that there was a significant amount of carbon and oxygen on the surface.

* Manuscript under preparation for Applied Surface Science by Cole et al.

The atomic composition of the main constituents was 45% carbon, 45% oxygen, 8% iron and 2% chromium. From the peak area analysis of the survey scan and based on the oxide stoichiometry, most of the oxygen was bound to iron and chromium as Fe_2O_3 or Cr_2O_3, while approximately 30% of the oxygen was bound to either carbon (COOH or COH groups) or hydrogen (OH, H_2O). Most of the carbon was either bound to other carbon atoms or to hydrogen, but the survey scan (see Figure 3.3) also showed a shoulder on the carbon 1s peak at 288 eV, indicating that some carbon was involved in bonding with oxygen or fluorine (e.g. CF_2, COH or COOH groups).

The high resolution Cr $2p_{3/2}$ signal of stainless steel required three peaks in the deconvolution for the best fit ($\chi^2 = 1.675$), with the metallic chromium peak located at 574.3 eV. If two peaks were used for fitting, per Rossi *et al.*,[18] the fit was not acceptable ($\chi^2 = 2.688$). Therefore, the hydroxide sub-peak was taken into consideration, as others have done.[65,66] Results of the Cr $2p_{3/2}$ peak from stainless steel show the chromium peak binding energy at 574.3 eV (2.00 eV FWHM), the chromium oxide peak was at 576.2 eV (2.27 eV FWHM) and the chromium hydroxide peak was at 577.6 eV (2.65 eV FWHM). An example of the data taken in this experiment with a three-peak fit is shown in Figure 6.1(a).

The high resolution scan of the O 1s peak, shown in Figure 6.1(b), was fit ($\chi^2 = 1.755$) with three sub-peaks for the oxide, hydroxide and water, as in the literature.[18,87] The O 1s peak had its main oxide sub-peak at 529.7 eV (1.30 eV FWHM), the hydroxide sub-peak at 531.1 eV (1.40 eV FWHM) and the water sub-peak at 532.2 eV (1.49 eV FWHM). The water sub-peak has been shown to

contribute at binding energy up to 534 eV,[67,87] but other publications agree with our interpretation.[18,66]

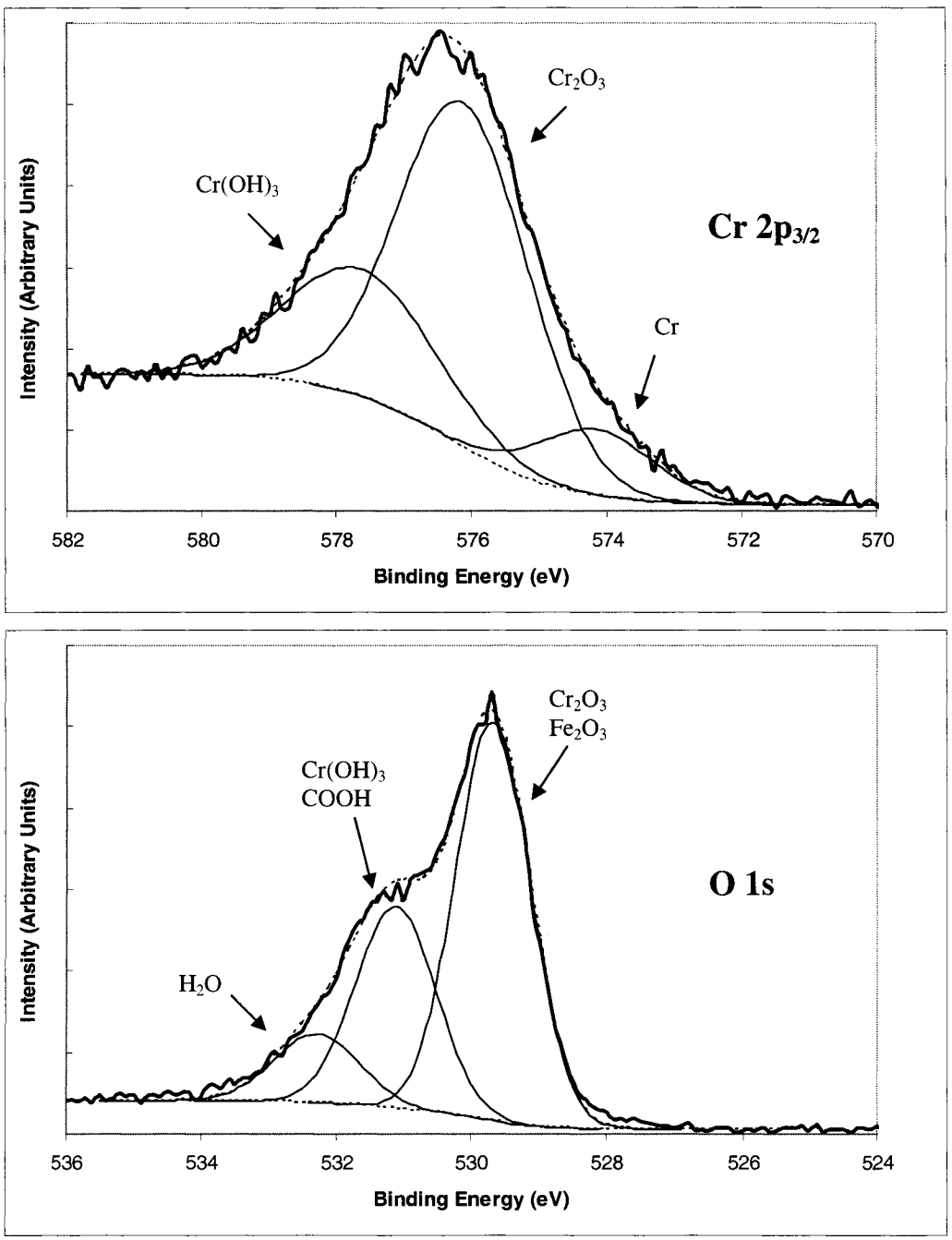

FIGURE 6.1 Deconvolution of Cr $2p_{3/2}$ peak (a) and O 1s peak (b) show three sub-peaks.

6.2 Fluorine Results and Discussion

Since fluorine is normally thought of as the source of mass 19 in mass spectrometers, it was interesting to note its contribution to the surface of stainless steel. Also, the effects of electron bombardment and heating were observed.

The high resolution scan of F 1s showed that a small amount of fluorine existed in the sample in two forms, with binding energies of 684 and 689 eV. The 689 eV peak indicates CF_x on the surface while the peak at 684 eV indicates metal fluorides at or near the surface. Because the F contribution was so small, a scan using the same parameters as the F 1s scan was done on the O 1s peak for comparison. The O 1s and F 1s peaks revealed that fluorine was only 0.8% as abundant as oxygen, and thus only 0.4% of the total surface/sub-surface composition.

As can be seen in Figure 6.2, the F 1s signal initially indicated two species existing at or near the surface, each containing about half the total amount. After electron bombardment, the surface F 1s signal at 689 eV disappeared while the sub-peak at 684 eV remained. Also, the C 1s signal at 288 eV (possibly CF_x) was reduced by the bombardment. After heating to 400 °C, the F 1s sub-peak at 684 eV disappeared and was not detected after cooling for an hour in vacuum and exposure to atmosphere for 8 hours.

When the stainless steel was bombarded with electrons, any fluorine that was bound to carbon on the surface was removed, but there was little effect on the metal fluorides. This is most likely because the fluorides are found below the surface, where electron stimulated desorption does not readily occur. Although, ESD ions can

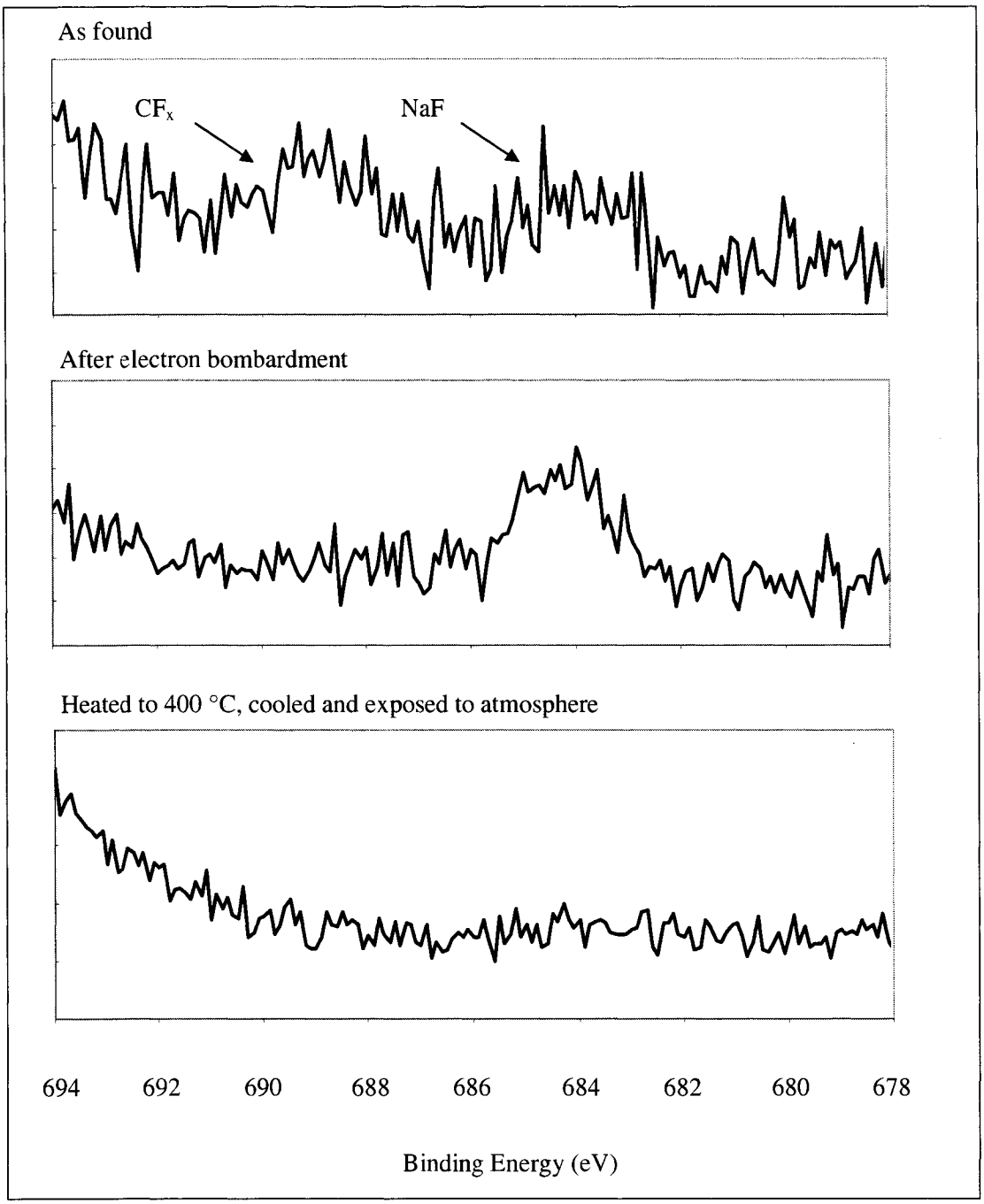

FIGURE 6.2 The XPS spectrum of F 1s shows that electron bombardment reduces surface fluorine compounds, but not bulk fluorine. Heating reduces both. The feature to the far left is contribution from the Cr 2s peak.

emanate from below the surface, the probability is reduced. For example, experiments have shown that ESD F^+ ion flux is reduced by 90% if it must pass through just two monolayers of water.[88]

When the steel is heated to 400 °C, the signal from the metal fluorides disappears and it does not return after cooling or after exposure to atmosphere for eight hours. This suggests that while there may be fluorides present initially, once they are eliminated they do not return. Therefore, there is little support for background accretion of fluorine causing the return of the signal at mass 19.

6.3 Heating and Hydrogen Dosing

In order to ascertain the source and behavior of hydroxides on the surface of stainless steel and chromium, samples were heated and dosed with hydrogen as described in section 3.6 and 3.6.1. Preliminary data were taken using polished stainless steel and chromium before and after heating to 400 °C for 3 hours, after accretion from the background overnight and after hydrogenation at 1×10^{-7} Torr for three hours. The contributions of each Cr $2p_{3/2}$ sub-peak in the stainless steel and in the chromium samples are shown in Table 6.1. After heating, the amount of hydroxide in the stainless steel decreased from 53% to 23%, but there was little change for the chromium sample. After accretion of hydrogen from the background vacuum overnight, there was an increase in hydroxides from 23% to 30% in stainless steel and from 9% to 20% in chromium. There were no discernable changes after further hydrogen dosing.

TABLE 6.1 Contribution of Cr 2p3/2 sub-peaks for stainless steel and chromium after various treatments.

	Polished Stainless Steel			Polycrystalline Chromium		
	Metal	Oxide	Hydroxide	Metal	Oxide	Hydroxide
Polished	3%	44%	53%	23%	69%	8%
Heated	12%	65%	23%	16%	75%	9%
Accretion/ Hydrogenated	20%	50%	30%	20%	60%	20%

Heating the stainless steel sample clearly segregates more chromium to the surface where it scavenges oxygen from iron. However, heating the polycrystalline chromium sample may actually allow the oxygen from the surface to diffuse deeper, reducing the percentage of metallic chromium in the signal.

Figure 6.3 shows the variation in atomic percentage of several species as the polished stainless steel sample was heated incrementally to 500 °C, as described in section 3.6.1. After initially decreasing from 31% to 6%, carbon begins increasing again above 300 °C to 24% at 500 °C. The oxygen begins decreasing from over 60% at 300 °C down to about 50% at 500 °C. The chromium content increases with temperature from its initial value of 2% to a value of 22% at 400 °C and above. The iron content increases from its initial value of over 8% to over 23% at 300 °C and then decrease to less than 4% at 400 °C and above. A small amount of manganese (< 4%) begins to show up at 400 °C. The increase in chromium and decrease in iron content were both expected, since this has been observed with other types of analysis, such as Auger electron spectroscopy.[31]

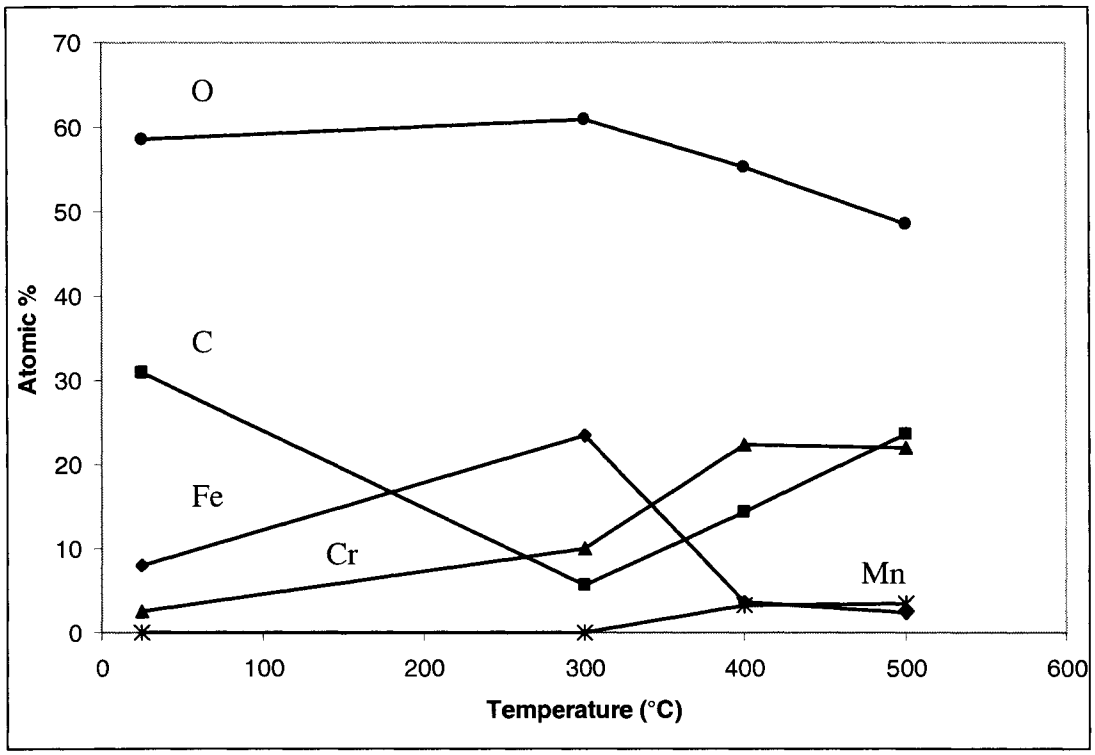

FIGURE 6.3 The surface composition of the 316L stainless steel varies as sample temperature changes.

The O 1s signal diminished with increasing temperature as water and hydroxides left the surface. High resolution scans of the O 1s peak showed that the shoulder on the peak also decreased, indicating a reduction in hydroxides. As received, the hydroxide and water contribution to the O 1s peak was over 30%. At 300 °C it dropped to 22% with no discernable water sub-peak. At 400 °C and 500 °C the hydroxide contributions were 16% and 8% respectively.

6.4 Electron bombardment

As discussed in Chapter V, since hydronium is generated by ESD as electrons strike the grid of mass spectrometers, XPS was used to study hydronium precursors on stainless steel and chromium as a function of electron bombardment. XPS spectra of the Cr $2p_{3/2}$ and O 1s peaks were collected from a stainless steel substrate after 5 hours and 8 hours of bombardment with 0.3 mA of 70 eV electrons. The same experiment was conducted for chromium except that electron bombardment was only done for 5 hours due to system time constraints.

The O 1s spectrum of stainless steel after 5 hours of electron bombardment is shown in Figure 6.4. The O 1s sub-peak at 529.7 eV (1.30 eV FWHM) was the largest and remained relatively unchanged, but increased its contribution to the overall signal from 57% to 77%. The peak at 531.1 eV (1.40 eV FWHM), corresponding to hydroxides and carboxyl groups, was reduced in height and its contribution to the O 1s signal changed from 32% to over 22%. The contribution of the shoulder at 532.2 eV (1.49 eV FWHM), corresponding to water and carbonyls, was reduced from 11% to < 1%.

In order to note changes to the Cr $2p_{3/2}$ peak, a larger pass energy value of 150 eV was used to increase the signal strength (see section 3.5.1). However, the signal was still very noisy and difficult to fit. The peak was composed of three sub-peaks at 574 eV, 576 eV and a broad shoulder at 577.9 eV. The contribution of the Cr $2p_{3/2}$ sub-peak from the Cr metal at 574 eV (2.00 eV FWHM) increased from 7% to 16%. The contribution of the sub-peak from chromium oxide at 576 eV (2.2 eV FWHM)

increased from 51% to 67%. Finally, the contribution of the sub-peak from chromium hydroxide at 577.9 eV (2.3 eV FWHM) decreased from 42% to 17%. This is consistent with hydroxides leaving the surface through H^+, OH^+ or H_3O^+ ESD.

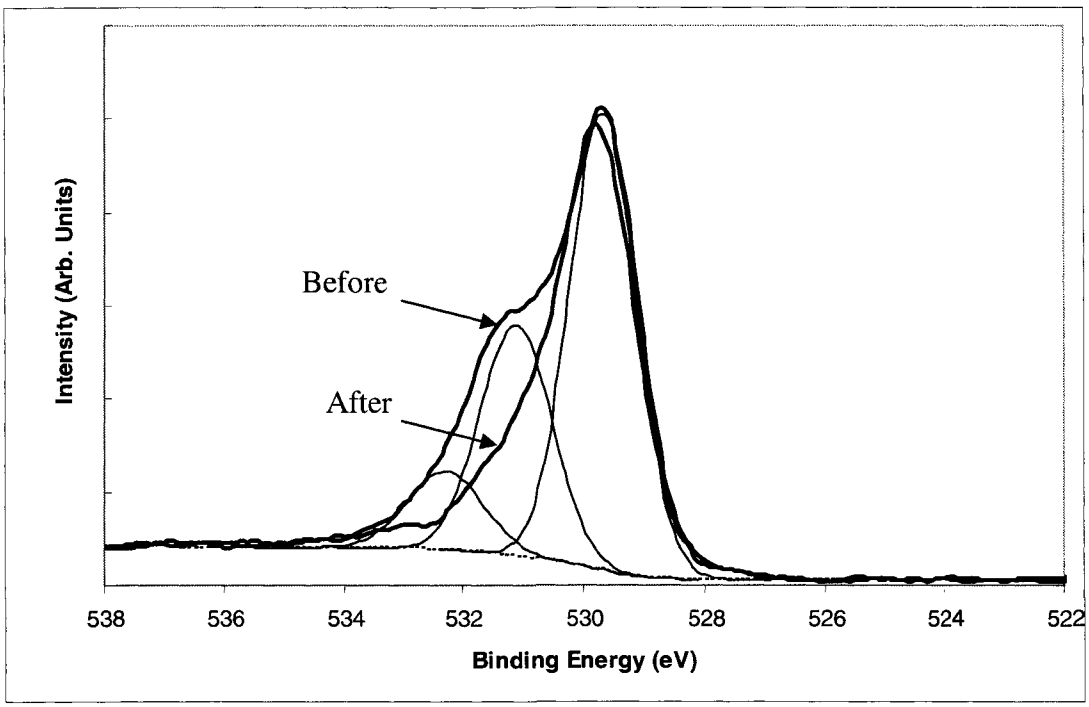

FIGURE 6.4 The O 1s peak shows a decrease of the shoulder at 531.1 eV after 70 eV electron bombardment at 0.3 mA for 5 hours.

Electron bombardment of the polycrystalline chromium sample increased the amount of the Cr $2p_{3/2}$ signal due to the oxide at 576.3 eV (2.27 eV FWHM) by 6% and reduced the signal from the metal at 574.5 eV (1.58 eV FWHM). The O 1s peak shows an increase in the oxide signal at 530.7 eV (1.46 eV FWHM) while the hydroxide and water signals at 532.1 eV (1.66 eV FWHM) and 533 eV (2.31 eV FWHM) decrease. These results are shown in Figure 6.5.

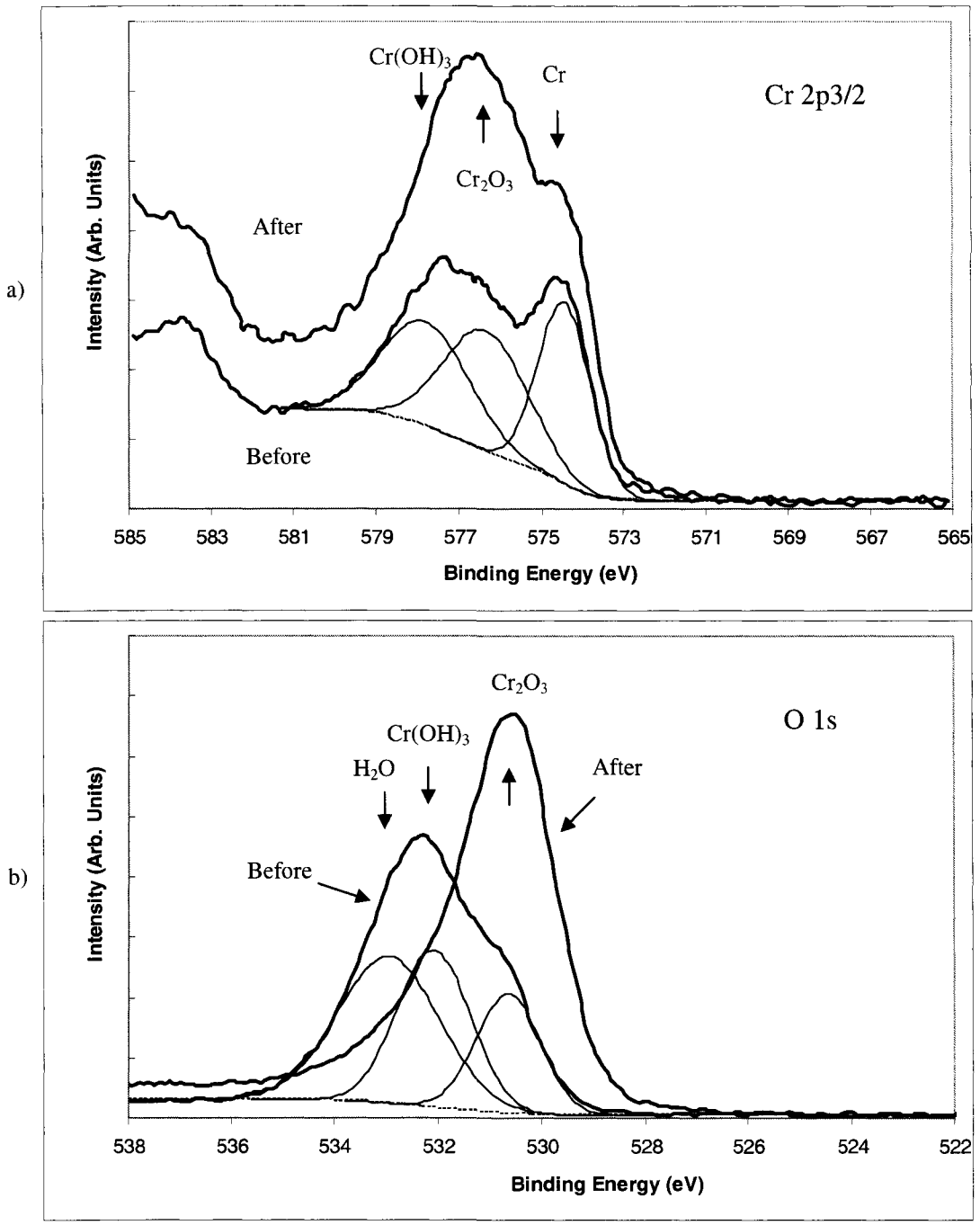

FIGURE 6.5 The Cr $2p_{3/2}$ peak (a) and O 1s peak (b) in polycrystalline chromium show an increase in the oxide and decrease in hydroxides after electron bombardment.

6.5 Discussion

As discussed in sections 2.3 and 2.7, it is generally accepted that the passive film of austenitic stainless steels is mostly a chromium hydroxide outer layer (~ 15 A) containing some iron hydroxide and a chromium oxide inner layer (20 – 40 A) with some iron oxide, chromium and iron. A schematic of the surface composition is shown in Figure 6.6. XPS and TOF-SIMS data support this conclusion, with TOF-SIMS unambiguously showing the presence of positive and negative ions of CrOH and FeOH.[18,65] A sub-layer is found below this passive layer containing chromium, iron and nickel oxides with some chromium, iron and nickel metal. Alloys with higher chromium content seem to have a thinner chromium oxide layer, but are more corrosion resistant. This is possibly because oxygen reacts with the chromium mostly on the surface leading to a dense film that retards inward diffusion of oxygen.[65]

Rossi[18] *et al.* suggested that the O 1s signal is comprised of three peaks at 530.0 ± 0.2 eV, 531.3 ± 0.25 eV and 532.7 ± 0.2 eV, which is consistent with our analysis. The three peaks have been attributed to Cr_2O_3, chromium hydroxide and water respectively.[18] In stainless steel it is likely that the component near 530 eV has a small contribution from Fe_2O_3, and CrO and FeO sub-oxides.

McCafferty *et al.*[87] point out that carboxyl (COOH) and carboxylate (COO) groups contribute to the shoulder as well. The component near 531 eV corresponds to COOH, Cr(=O)OH and $Cr(OH)_3$, and the component near 532 eV is assigned to H_2O and possible ester oxygen (O–C=O) in those carboxyl groups.

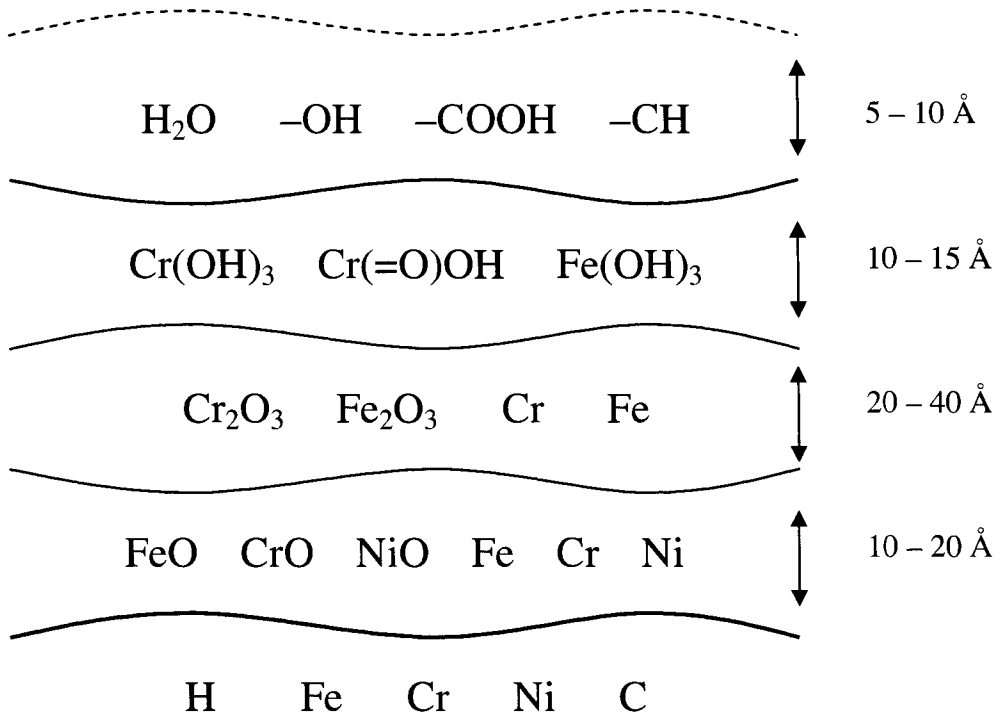

FIGURE 6.6 A schematic showing the chemistry of the surface of stainless steel.

Hydrogen dosing the samples generated the formation of hydroxides at the surface, but not to a great extent. The amount of water formation on the surface depends linearly on the amount of hydrogen present and the temperature of the surface. If the surface is heated to 900 °C in an oxygen atmosphere, its ability to produce water is reduced.[62] This is no doubt due to the fact that no hydrogen is available to be incorporated into the oxide. Hot filaments in ion sources would promote the formation of very reactive atomic hydrogen that could interact with the grid oxide layer.[89]

The source of oxygen for hydroxides and, ultimately, hydronium, is most likely surface oxides or carbon oxides. In the case of surface oxides, Cr_2O_3 is so strongly bound and stable (enthalpy of formation = -269.7 kcal/g/mol) that it is seen as a less likely candidate for the source of oxygen than iron oxides or nickel oxides. Since heating segregates more chromium to the surface of stainless steel, the evidence of reduced water formation supports this hypothesis,[62] although other stainless steel constituents could contribute. The enthalpy of reaction at 400 °C for reduction of NiO to Ni is -8 kJ/mol-H_2O, compared to 34 kJ/mol-H_2O for Fe_3O_4 to Fe and 102 kJ/mol-H_2O for Cr_2O_3 to Cr.[63] Enthalpies for FeO (272 kJ/mol) and Fe_2O_3 (825.5 kJ/mol) [90] are lower than those for CrO (429.3 kJ/mol) and Cr_2O_3 (1128.4 kJ/mol).[91] Therefore, it would seem that hydroxide formation from nickel or iron oxides is more thermodynamically favorable. Heating also promotes the formation of a more ordered oxide, leaving fewer defect sites for formation. These defects play an important role in causing water dissociation and hydroxyl formation on the oxide surface.[60] Nevertheless, the thermal vacuum processes also result in diffusion of bulk hydrogen to the surface complex that ultimately forms hydroxides and probably hydronium.

Other metals may have the capability of generating water and hydronium from hydrogen, oxygen and hydroxides as well. Co-adsorption of hydrogen with oxygen on palladium can have various structures depending on temperature.[64] These structures change between a (2×2) ordered phase and a $(\sqrt{3} \times \sqrt{3})$ phase as hydrogen diffuses in and out of the bulk. Above 220 K, oxygen is lost from the Pd surface due to formation of OH and, subsequently, H_2O as hydrogen segregates from the bulk.[64]

When the stainless steel is bombarded with electrons, the sub-peak at 531 eV (COOH, $Cr(OH)_3$) and the shoulder at 532 eV (H_2O) are reduced. The hydroxides and carboxyl contaminants on the surface desorb as CO, H_2, H^+ and H_3O^+ and allow more sub-surface CrO, FeO and Fe_2O_3 to be detected.

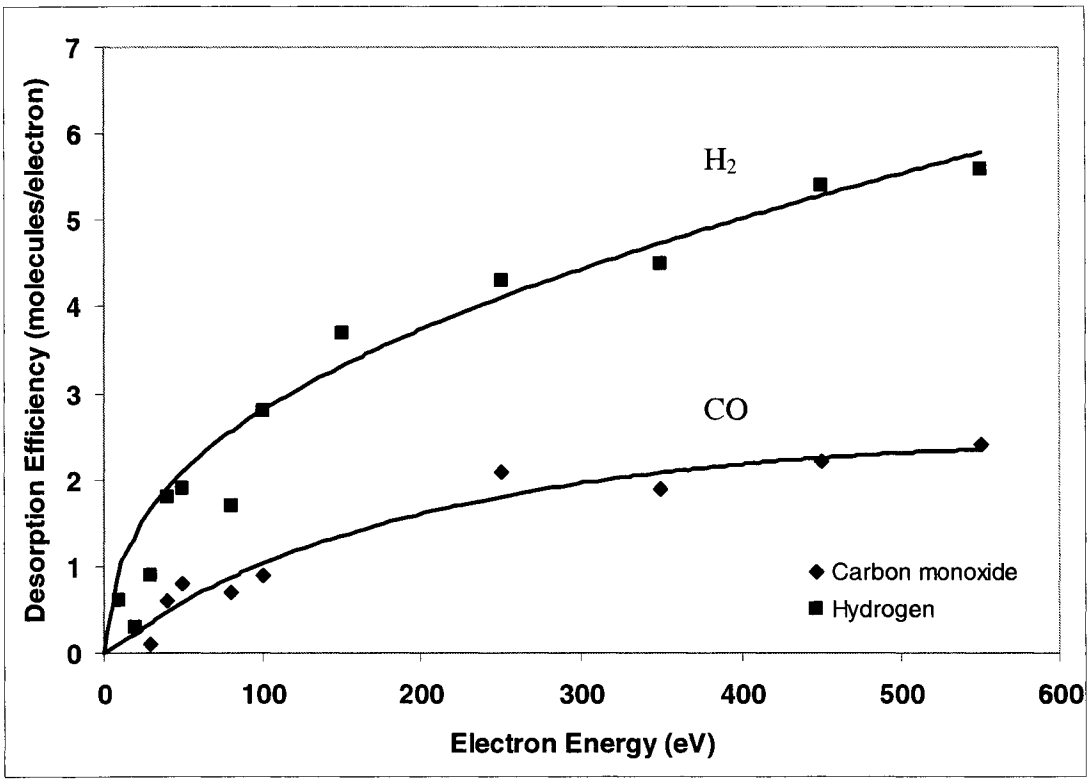

FIGURE 6.7 The desorption efficiency of CO and H_2 increase as electron energy increases, with hydrogen being the most significant gas desorbed.[92]

Related work in Figure 6.7 shows the desorption efficiency of H_2 and CO desorbed by ESD/thermal mechanism following heating of a polished stainless steel surface.[92] As the voltage was increased, the desorption flux also increased, but did not reach a maximum. The desorption of a significant quantity of both H_2 and CO is

consistent with the diminution of both O and H on the surface.[31] Although heating to 400 °C is sufficient to remove all adsorbed water, electron bombardment showed the most significant gas desorbed was still H_2. The surface was most likely re-supplied by hydrogen diffusion from the bulk which may ultimately form hydroxides. Additionally, the ESD of CO could leave "free" OH (from COOH, for example) that interacts with existing hydroxides to form H_3O^+ via ESD.

Another possibility to consider is that some $Cr(OH)_3$ or $Cr(=O)OH$ is converted to Cr_2O_3 or CrO_2 as the shoulder at 531 eV reduces, since the chromium to oxygen ratio would decrease. These conversions are supported by the chromium data in Figure 6.5, since the hydroxide and Cr metal signals reduce while the oxide peak increases during bombardment. We propose reactions given by

$$Cr(OH)_3 + e^- \rightarrow CrO_2 + H_3O^+ + 2e^- \qquad (6.1)$$

or

$$H + 2Cr(=O)OH + e^- \rightarrow 2CrO_2 + H_3O^+ + 2e^- \qquad (6.2)$$

However, it may be that electron bombardment just promotes the formation of Cr_2O_3 from chromium while also reducing hydroxides.

6.6 ESD model for H_3O^+

The precursors for hydronium formation are most likely hydroxides formed by the interaction of the protective oxide layer with hydrogen from the residual gas background and the bulk hydrogen that diffuses to the surface. Hydroxide formation can also be promoted by nearby hot filaments where atomic hydrogen can be created.[89] Further interactions with hydrogen and electrons may also lead to water and hydronium formation, as proposed by the following equations.

$$H_2 + Cr(OH)_3 \rightarrow Cr(OH)_2 + H_2O + H \qquad (6.3)$$

$$Cr(OH)_2 + H_2O + H + e^- \rightarrow Cr(OH)_2 + H_3O^+ + 2e^- \qquad (6.4)$$

Souda's work[17] with D_2O adsorbed on rare gas substrates showed emission of D_3O^+ ESD ions and higher order clusters ($D_5O_2^+$, etc.). In that work, it was also pointed out that previous studies using metal substrates did not have significant positive ion emission except for H^+. The reason for the limited emission is due to the delocalization of valence holes because of strong interactions between the water molecules and the metal substrate. On a rare gas substrate, isolated free clusters can be supported for long enough time periods so that Coulombic repulsion between valence holes can occur.[17] These valence holes are a result of Auger decay of deep core holes or multiple electron excitations. It is proposed that the protective oxide layer that naturally forms on the surface of stainless steel will inhibit delocalization of

valence holes created during electron bombardment. Defects in the oxide provide potential activation sites where hydrogen, hydroxides and water can interact to form hydronium.

There is also the possibility that a two-electron process can occur. A free O-H bond on the surface could yield an H^+ ion or the proton could travel along the axis of a hydrogen bond with a neighboring molecule and form hydronium. The available kinetic energy could free the H_3O^+ ion or a second electron could free the H_3O^+ molecule through the Knotek-Feibelman mechanism, described in section 2.2. It is even possible that formic acid (HCOOH) could form on the surface and become a source of H^+ ions.

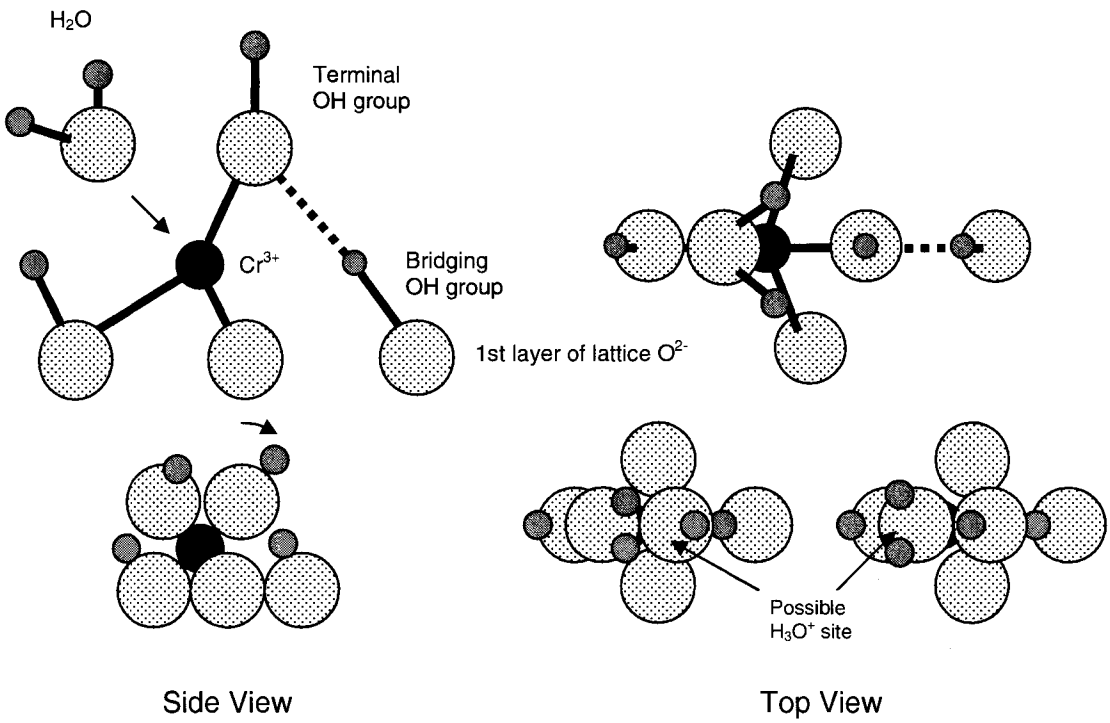

FIGURE 6.8 Schematic representation of Cr_2O_3 (001) surface with hydroxide groups. The additional bonding site for water could lead to hydronium formation.

The hydronium formation could be aided by the geometry of hydroxyl binding on the surface. As described by Henderson and Chambers,[67] and shown in Figure 6.8, an isolated terminal O-H bond and a bridging O-H bond on Cr_2O_3 can be involved in an unusually strong hydrogen bond. The Cr^{3+} cation involved with the terminal O-H group can also bind another non-dissociated molecule of water, facilitating hydronium formation.

Certainly, there are adequate sources for hydronium formation on stainless steel found in the form of surface hydroxides, surface oxides, hydrogen and water in the residual gas background and bulk hydrogen. Heating was shown to reduce the amount of surface hydroxides and water, while hydrogen dosing increased hydroxide formation. The interaction of electrons with the chromium oxide passive layer of stainless steel reduced the hydroxide content as well. These results support the findings in a QMS, where hydrogen dosing increased the ESD signal of hydronium and electron bombardment reduced the signal.

CHAPTER VII

SUMMARY

The data presented here indicate that the 19 amu peak observed in the residual gas spectra of a Fourier transform mass spectrometer (FTMS) is predominantly H_3O^+ rather than F^+ and its magnitude is strongly connected with the partial pressure of water. While, obviously, this observation of hydronium dominance may not be the norm if one is working with vacuum systems containing fluorine bearing gases, it is proposed that it makes up the predominant signal at mass 19 in systems without fluorine exposure. It has also been shown that there is sufficient time available in a quadrupole mass spectrometer (QMS) for secondary ion-molecule interactions to occur at pressures above 10^{-9} Torr leading to the formation of H_3O^+.

Using high resolution FTMS, high sensitivity QMS and time of flight secondary ion mass spectrometry (TOF SIMS), it has been shown that, in positive ion spectra, the mass 19 signal is predominantly H_3O^+. By varying electron emission current and H_2O partial pressure, it was shown that in ultrahigh vacuum (UHV), the H_3O^+ is generated by electron stimulated desorption (ESD) at the grid, independent of adsorbed H_2O. As the partial pressure of water increases from 4×10^{-10} Torr, the mass 19/18 ratio decreases and then approaches a constant at pressures greater than $\sim 1 \times 10^{-9}$ Torr. The ESD generated H_3O^+ signal is relatively unaffected by hydrogen dosing at modest exposures, but increases by a factor of 10 upon saturation hydrogen

exposure for 8 hours. Consistent with a surface electron ESD process, the H_3O^+ signal then rapidly decays with the depletion of surface hydrogen.

As the partial pressure of H_2O^+ increases above ~1×10^{-9} Torr, the ratio of mass 19 to mass 18 in the QMS becomes a constant (~ 0.04), suggesting a dependence on adsorbed water. As the pressure reaches 1×10^{-7} Torr, gas phase collision mechanisms become the dominant H_3O^+ source.

Since ESD surface ions from stainless steel are frequently seen, but often ambiguous, XPS was used to determine the effects of heating, electron bombardment and hydrogen dosing on hydroxides and fluorine in stainless steel and chromium. The H_3O^+ generated by ESD could be connected with a surface complex, possibly a metal hydroxide. From the data presented in Chapter VI it is clear that fluorine and hydroxides are present on the stainless steel surface. Fluorine is not abundant and electron bombardment is only effective in removing fluorine found in complexes on the surface, not in the bulk material. However, heating the sample eliminates the remaining fluorine signal, including metal halides below the surface. Re-exposure to ambient did not re-introduce F onto the metal surface. These observations run contrary to what other researchers have claimed to notice about the behavior of fluorine.

The O 1s peak was shown to be made up of three sub-peaks, one corresponding to chromium and iron oxides, another to chromium hydroxide and carboxyl groups and one to water and carbonyl groups. The Cr $2p_{3/2}$ peak consists of chromium, chromium oxide and chromium hydroxide sub-peaks. Heating the stainless steel reduces the amount of hydroxides and hydrogen dosing promotes a

limited increase in their abundance. This supports the results of hydrogen dosing the grid of a QMS where the signal from mass 19 increased.

Electron bombardment of both stainless steel and chromium surfaces reduces hydroxides as indicated by the decrease in the hydroxide shoulder on the O 1s and Cr $2p_{3/2}$ peaks. It is believed that this reduction occurs through ESD of H_2, OH, H^+ and H_3O^+. Again, this result follows logically, since the mass 19 signal decays during electron bombardment of the grid in a QMS. Electron bombardment also increases the chromium oxide signal.

Through this study we have seen that the presence of a mass 19 amu peak in a mass spectrometer is predominantly H_3O^+ rather than fluorine. Using various forms of mass spectrometry and surface analysis has allowed us to see how this anomalous mass spectral peak might arise. The hydronium formation occurs through electron stimulated desorption via surface interactions with the residual gas background, and the process can be enhanced by the presence of water vapor and hydrogen. Certainly, we have shown that it would be beneficial to use additional analysis techniques to better understand and explore other anomalous signals that one might see in mass spectra.

REFERENCES

[1] W. L. Fite and P. Irving, J. Vac. Sci. Technol. **11** (1), 351 (1974).

[2] P. A. Redhead, J. Vac. Sci. Technol. **7** (1), 182 (1969).

[3] C. R. Cole, R. A. Outlaw, R. L. Champion, D. H. Baker, and B. C. Holloway, J. Vac. Sci. Technol. A **21** (5), 1796 (2003).

[4] R. E. Ellefson, in *Foundations of Vacuum Science and Technology*, edited by J. M. Lafferty (Wiley, New York, 1998).

[5] J. F. O'Hanlon, *A Users Guide to Vacuum Technology*, 2nd ed. (John Wiley & Sons, New York, 1998).

[6] M. J. Drinkwine and D. Lichtman, *Partial Pressure Analyzers and Analysis.* (The Education Committee of the American Vacuum Society, New York, 1980).

[7] Stanford Research Systems, Choosing a Quadrupole Gas Analyzer, Application Note No. 9, 2005

[8] Stanford Research Systems, Vacuum Diagnosis with a Residual Gas Analyzer, Application Note No. 7, 1996

[9] J. P. Adrados and J. L. de Segovia, Vacuum **34** (8-9), 737 (1984).

[10] J. H. Neave and B. A. Joyce, J. Phys. D: Appl. Phys. **9** (15), 2195 (1976).

[11] C. R. Cole, R. A. Outlaw, R. L. Champion, D. H. Baker, and B. C. Holloway, J. Vac. Sci. Technol. A **22** (5), 2056 (2004).

[12] M. J. Drinkwine and D. Lichtman, J. Vac. Sci. Technol. **15** (1), 74 (1978).

[13] R. Schubert, J. Vac. Sci. Technol. **12** (1), 505 (1975).

[14] D. Lichtman, J. Vac. Sci. Technol. **2** (2), 91 (1965).

[15] R. Schubert, J. Vac. Sci. Technol. **11** (5), 903 (1974).

[16] H. D. Beckey, *Principles of Field Ionization and Field Desorption Spectrometry*, First ed. (Pergamon Press, Oxford, 1977).

[17] R. Souda, Surf. Sci. **511** (1-3), 147 (2002).

[18] A. Rossi, B. Elsener, G. Hahner, M.Textor, and N. D. Spencer, Surf. Interface Anal. **29**, 460 (2000).

[19] B. V. Yakshinskiy and T. E. Madey, Nature **400** (6745), 642 (1999).

[20] T. E. Madey and J. T. Yates, J. Vac. Sci. Technol. **8** (4), 525 (1971).

[21] D. Lichtman, Surf. Sci. **90** (2), 579 (1979).

[22] D. Menzel and R. Gomer, J. Chem. Phys. **41**, 3311 (1964).

[23] P. A. Redhead, Can. J. Phys. **42**, 886 (1964).

[24] M. L. Knotek and Peter J. Feibelman, Phys. Rev. Lett. **40** (14), 964 (1978).

[25] P. Williams and G. Gillen, Surf. Sci. Lett. **180** (1), L109 (1987).

[26] M. L. Knotek, V. O. Jones, and V. Rehn, Phys. Rev. Lett. **43** (4), 300 (1979).

[27] G. W. Fabel, S. M. Cox, and D. Lichtman, Surf. Sci. **40** (3), 571 (1973).

[28] R. N. Peacock, in *Foundations of Vacuum Science and Technology*, edited by J. M. Lafferty (Wiley, New York, 1998).

[29] F. Watanabe, J. Vac. Sci. Technol. A **20** (4), 1222 (2002).

[30] H. Pfnur and D. Menzel, J. Chem. Phys. **79**, 2400 (1983).

[31] R. A. Outlaw, Z. Xin, B. C. Holloway, M. R. Davidson, and E. Lambers, Appl. Surf. Sci. **227**, 7 (2004).

[32] S. Rezaie-Serej and R. A Outlaw, J. Vac. Sci. Technol. A **12**, 2814 (1994).

[33] C.E. Tripa and Jr. J.T. Yates, Nature **398**, 591 (1999).

[34] J. T. Yates and D. A. King, J. Vac. Sci. Technol. **9** (5), 1256 (1972).

[35] G. R. Floyd and R. H Prince, Surf. Sci. **59**, 631 (1976).

[36] M. B. Jensen, J. S. Dyer, W. Y. Leung, and P. A. Thiel, Langmuir **12** (14), 3472 (1996).

[37] M. A. B. De Moraes and D. Lichtman, Surf. Sci. **160** (2), 362 (1985).

[38] M. de Moraes and D. Lichtman, J. Vac. Sci. Technol. A **2** (4), 1595 (1984).

[39] C. Park, M. Kramer, and E. Bauer, Surf. Sci. Lett. **109**, L533 (1981).

[40] K. Miura, Solid State Commun. **94**, 243 (1995).

[41] T. E. Madey and J. T. Yates, Surf. Sci. **63**, 203 (1977).

[42] Ph. Avouris, R. Kawai, N. D. Lang, and D. M. Newns, J. Chem. Phys. **89** (4), 2388 (1988).

[43] J. A. Yarmoff and S. A. Joyce, Phys. Rev. B **40**, 3143 (1989).

[44] J. A. Yarmoff, Taleb-Ibrahimi, F. R. McFeely, and Ph. Avouris, Phys. Rev. Lett. **60**, 960 (1988).

[45] D. P. Woodruff, M. M. Traum, H. H. Farrell, N. V. Smith, P. D. Johnson, D. A. King, R. L Benbow, and Z. Hurych, Phys. Rev. B **21** (12), 5642 (1980).

[46] M. D. Scheer, R. Klein, and J. D. McKinley, Surface Sci. **30**, 251 (1972).

[47] M. Nishijima and F. M. Propst, J. Vac. Sci. Technol. **7**, 410 (1970).

[48] S. R. Baggott, K. W. Kolasinski, L. M. A. Perdigao, D. Riedel, Guo Quanmin, and R. E. Palmer, J. Chem. Phys. **117** (14), 6667 (2002).

[49] J. F. Shackelford, *Introduction to Materials Science for Engineers*, 4th ed. (Prentice-Hall, Upper Saddle River, 1996).

[50] World Wide Web, http://chemistry.about.com, 2005

[51] World Wide Web, http://www.lsbu.ac.uk/water/explan.html, 2005

[52] R. A. Langley, *Lesson 6: The Scourge of Vacuum Systems*, Vacuum Technology and Coating, April 2005, p. 52

[53] W. Lindinger, Int. J. of Mass Spectrom. **173**, 191 (1998).

[54] C. Clay, S. Haq, and A. Hodgson, Phys. Rev. Lett. **92** (4), 046102/1 (2004).

[55] D. Menzel, Science **295**, 58 (2002).

[56] P. Feibelman, Science **295**, 99 (2002).

[57] R. Ludwig, Angew. Chem. Int. Ed. **42**, 3458 (2003).

[58] L. J. Michot, F. Villieras, M. Francois, I. Bihannic, M. Pelletier, and J. Cases, Comptes Rendus Geosciences **334**, 611 (2002).

[59] J. Yang, S. Meng, L. F. Xu, and E. G. Wang, Phys. Rev. Lett. **92**, 146102 (2004).

[60] T. Bredow, Surf. Sci. **401** (1), 82 (1998).

[61] H. Hunt, BJM Stainless Group Pty Ltd., 2000

[62] L. C. Beavis, J. Vac. Sci. Technol. **10** (2), 386 (1973).

[63] H. Funke, J. Yao, and M. W. Raynor, J. Vac. Sci. Technol. A **22** (2), 437 (2004).

[64] T. Mitsui, M. K. Rose, E. Fomin, D. F. Ogletree, and M. Salmeron, Surf. Sci. **511**, 259 (2002).

[65] G. Lothongkum, S. Chaikittisilp, and A. W. Lothongkum, Appl. Surf. Sci. **218** (1-4), 202 (2003).

[66] V. Maurice, S. Cadot, and P. Marcus, Surf. Sci. **471**, 43 (2001).

[67] M. A. Henderson and S. A. Chambers, Surf. Sci. **449** (1-3), 135 (2000).

[68] V. Maurice, S. Cadot, and P. Marcus, **458** (1-3), 195 (2000).

[69] H. A. Bullen and S. J. Garrett, Surf. Sci. Spectra **8** (3), 225 (2001).

[70] F. T. Wagner and T. E. Moylan, Surf. Sci. **206**, 187 (1988).

[71] S. Badilescu and C. Sandorfy, Can. J. of Chem. **65** (5), 924 (1987).

[72] P. Blowers, N. Chen, and R. I. Masel, J. Vac. Sci. Technol. A **17** (4), 1750 (1999).

[73] I. J. Amster, J. Mass Spectrom. **31**, 1325 (1996).

[74] A. G. Marshall, C. L. Hendrickson, and G. S. Jackson, Mass Spectrom. Rev. **17**, 1 (1998).

[75] W. Paul, H. P. Reinhart, and U. von Zhan, Z. Phys. **152**, 143 (1958).

[76] C. Richard Brundle, Charles A. Jr. Evans, and Shaun Wilson, (Butterworth-Heinemann (Elsevier), Boston, 1992).

[77] Stanford Research Systems, SRS RGA Version 2.0 Library (1996).

[78] R. C. Bolden and N. D. Twiddy, Faraday Discuss. Chem. Soc. **53**, 192 (1972).

[79] R. A. Fluegge, J. Chem. Phys. **50**, 4373 (1969).

[80] S. K. Gupta, E. G. Jones, A. G. Harrison, and J. J. Myher, Can. J. of Phys. **45**, 3107 (1967).

[81] G. Lawson, R. F. Bonner, R. E. Mather, J. F. J. Todd, and R. E. March, J. Chem. Soc.: Faraday Trans. 1 **72**, 545 (1976).

[82] J. Vancura and Z. Herman, Chem. Phys. **151**, 249 (1991).

[83] M. M. Traum and D. P. Woodruff, J. Vac. Sci. Technol. **17** (5), 1202 (1980).

[84] M. H. Drinkwine and D. Lichtman, Progress in Surf. Sci. **8** (3), 123 (1977).

[85] H. D. Beckey, Z. Naturf **14a**, 712 (1959).

[86] L. H. Anderson, O. Heber, D. Kella, H. B. Pedersen, L. Vejby-Christensen, and D. Zajfman, Phys. Rev. Lett. **77** (24), 4891 (1996).

[87] E. and Wightman McCafferty, J. P., Surf. Interface Anal. **26**, 549 (1998).

[88] M. Akbulut, N. J. Sack, and T. E. Madey, **28** (7-8), 177 (1997).

[89] R. Erlandsson, Applications of Surf. Sci. **6** (3-4), 473 (1980).

[90] D. Ebbing, *General Chemistry*, 3rd ed. (Houghton-Mifflin, 1990).

[91] *CRC Handbook of Chemistry and Physics*, 60th ed. (CRC Press, Boca Raton, 1979).

[92] R. A. Outlaw, Unpublished work.

VITA

Charles Randal Cole

Charles Randal Cole was born in Newport News, Virginia on June 24, 1973. He graduated as salutatorian from Kecoughtan High School in Hampton, Virginia in June of 1991. Randy Cole received his Bachelor of Science in Electrical Engineering with a minor in Physics from Old Dominion University in Norfolk, Virginia in December of 1996. He continued on at ODU to receive his Master of Science in Electrical Engineering with an emphasis in Physical Electronics in December of 1997.

In June 1997, prior to completing his Master's degree, Randy began working as a Project Engineer at Teledyne Hastings Instruments in Hampton, Virginia. While working at Teledyne, Randy entered the Applied Science department of The College of William and Mary in September of 1998. He defended his dissertation in November of 2005. He continues to work at Teledyne serving as a project leader developing gas flow control and vacuum pressure measurement instrumentation.